Alma Mater Studiorum · Università di Bologna

SCUOLA DI SCIENZE

Corso di Laurea Magistrale in Matematica

Mathematical models in biomedicine

Tesi di Laurea Magistrale in Analisi Matematica

Relatore:
Chiar.mo Prof.
Maria Carla Tesi

Correlatore:
Dott. Luca Meacci

Presentata da:
Claudia Maggiori

Sessione Unica
Anno Accademico 2019-2020

Contents

List of Figures

Sommario

In questa tesi vengono innanzitutto presentati due metodi matematici per lo studio di modelli biomedici e comportamentali. I modelli presentati sono tre: un modello per lo studio dell'evoluzione della malattia di Alzheimer, uno per lo studio dello sviluppo dei tumori e uno per la diffusione del Covid-19. Si riportano anche alcuni codici utilizzati per lo studio e lo sviluppo dei modelli trattati. Le conclusioni contengono alcuni possibili sviluppi degli argomenti trattati.

Introduction

The art of applying mathematics to real problems, be they in engineering, biology, medicine, industry or any other discipline, is one that is of enormous importance. In particular, in recent decades, mathematics aimed at biomedicine has become a real interdisciplinary science.

First of all, what is a mathematical model? A model is a representation of a process [22]. Usually, a mathematical model takes the form of a set of equation describing a number of variables. The purpose of the model is to formulate a description of the considered phenomena in quantitative terms; the analysis of the resulting model leads to results that can be tested against the observations. Ideally, the model also leads to previsions which, if verified, support the authenticity of the model. It is important to realize that all models are idealizations, so their applicability is restricted. In fact, one usually aims to over-simplify; the idea is that, if the model is basically right, then it can be made more complicate, but its analysis is simplified by having treated a simpler version first [22].

Studying mathematical models is not so simple. Sometimes it is not possible to have an exact solution because the process could be very complicated. In this cases mathematical analysis provides a qualitative study of the solutions, while explicit ones are calculated via numerical methods. We separate continuous models, in which the variables vary continuously in space and time, and discrete models, whose variables varies discontinuously. This thesis deals only with the first case. In practice we will formulate models in terms of ordinary differential equations [22] and cellular automata [25]. Using ordinary differential equations we describe phenomena only in time, while with the cellular automata approach we can also take into account spatial features.

The first chapter of this thesis illustrates how to make a qualitative analysis of a system of autonomous ODE, and in particular how to study its local stability by applying the Routh-Hurwitz criterion [1], [3], [2].

Since, in addition to temporal evolution, we are also interested in phenomena of spatial nature, in the second chapter the Cellular Automata method is described [25]. This approach allow us to treat in some way pathologies such as Alzheimer's disease and tumors. It also allows to keep track of movements of people belonging of different categories, which will be useful to implement a new model for the study of Covid-19 epidemic described in Chapter 3.

The third chapter contains the presentation and analysis of three biomedical models, studied with the methods previously described.
The first model concerns Alzheimer's disease [40], [41], [14]. The system of ODE presented models the variation of Amyloidβ, a protein produced by neurons in healthy brains, which accumulates abnormally in presence of the disease. The solutions of this system allow to update the evolution of the illness, by a Cellular Automata approach, which is controlled in terms of a parameter varying between 0 and 1.
The second model deals with the expansion of a tumoral mass fomed by two types of cells: the cancer steam cells and the steams cells [13]. It takes also into account the tumor growth paradox [13], [45], [46], [47] and faces this mechanism with an ODE model. It also shows the tumor grotwth with a Cellular Automata approach.
After having studied these models, we tried to construct a new one. This new model represents the Covid-19 epidemic: it could eventually help government in taking decisions, because the model enables to predict future scenaries. As the cases above, for modelling the transmission mechanism we propose two approaches: the ODE and the Cellular Automata. Each model has its own introduction, which deeply explains the modelled mechanisms.

The fourth chapter contains the mathematical schemes used to analyze the models described above. In particular, these schemes are useful for the reader, because they allow to better understand the Cellular Automata mechanism.

Obviously, other aspects of the models presented can be studied, so the fifth chapter contains a summary and some new ideas that can be developed in future.

Chapter 1

Stability of systems of autonomous ODE

Autonomous non-linear systems of ordinary differential equations (ODE) allow to model and analyze natural phenomena. Often they are very difficult to solve and frequently classical solutions cannot be found. In order to deal with difficulties, one possible strategy consists in analyzing their stability.

1.1 The general case

Consider the following autonomous non-linear system:

$$\dot{x} = f(x) \tag{1.1}$$

with $f : \Omega \subset \mathbb{R}^n \to \mathbb{R}^n$. Suppose $f \in C^1(\Omega)$. Given $x_0 \in \Omega$, the map $t \to \phi^t(x_0) \in \Omega$ from $I \subset \mathbb{R}$ to Ω indicates the solution of the Cauchy's problem

$$\begin{cases} \dot{x} = f(x) \\ x(0) = x_0 \end{cases}$$

Definition 1.1. $a \in \Omega$ is called equilibrium point for the system $\dot{x} = f(x)$ if $f(a) = 0$. The set $C_f = \{a \in \Omega; f(a) = 0\}$ is the set of the equilibrium points.

Definition 1.2. a is called stable in the sense of Lyapunov if $\forall\ \epsilon > 0\ \exists\ \delta_\epsilon > 0$ such that, if $\|x_0 - a\| < \delta_\epsilon$, results

- $\phi^t(x_0)$ is defined $\forall t \geq 0$,
- $\|\phi^t(x_0) - a\| < \epsilon\ \forall t \geq 0$.

Observation 1. This means that $\forall\ U$ neighborhood of a there exists a neighborhood $V \subset U$ such that each solution which starts from inner points of V remains in U for $t > 0$.

Definition 1.3. a is called asimptotically stable if it is stable and moreover $\lim_{t\to+\infty} \phi^t(x_0) = a$. a is called unstable if it is not stable.

Observation 2. 'Unstable' means that there exist at least one solution starting nearby a but not remaining close to a.

In order to study the stability of an equilibrium point of (1.1), one possibility is to analyze the stability of the linearized system, obtained via Taylor's formula. Given $a \in C_f$ and $f \in C^1$, writing $f(x) = f'(a)(x-a)+o(\|x-a\|)$, where $f'(a)$ is the jacobian matrix of f in a, we can relate the stability of a for the system $\dot{x} = f(x)$ to the stability of the linear system $\dot{x} = f'(a)x$.

Observation 3. If a is an equilibrium point for (1.1), consider the translation $z(t) = x(t) - a$. The equation (1.1) becomes

$$\dot{z}(t) = f(z(t) + a), \tag{1.2}$$

so, the solution $z(t) = 0$ of (1.2) corresponds the solution $x(t) = a$ of (1.1) and vice versa. This means that we can always refer to the origin as the equilibrium point.

1.2 The linear case

In this section we examine the stability of the linear autonomous system

$$\dot{x} = Ax \tag{1.3}$$

where $A \in M_{n\times n}(\mathbb{R})$ and $x \in \mathbb{R}^n$. For this aim, we must calculate the eigenvalues of A by solving the characteristic equation $\det(A - \lambda I) = 0$. Once eigenvalues are known, the following theorem can be used.

Theorem 1.2.1. *Let* $\lambda_j, \quad j = 1, \ldots, k$ *be the eigenvalues of the matrix A. Then the origin is*

- *a globally asimptotically stable equilibrium point if and only if the real part of each eigenvalue is negative, that is* $Re\lambda_j < 0 \quad for \quad j = 1, \ldots, k,$
- *a stable equilibrium point, but not asymptotically stable, if and only if* $Re\lambda_j \leq 0$ *and the eigenvalues with vanishing real part verify* $m_a(\lambda_j) = m_g(\lambda_j),$
- *unstable otherwise.*

Here $m_a(\lambda_j)$ *indicates the algebraic multiplicity of* λ_j*, while* $m_g(\lambda_j)$ *indicates its geometric multiplicity.*

For the proof see [4]

1.3 Routh-Hurwitz criterion

Definition 1.4. A characteristic polynomial which has only roots corresponding to asymptotically stable zeros of the system is called Hurwitz polynomial [3].

Now, we need to understand how to verify when a polynomial is a Hurwitz's polynomial. The following theorem help us.

Theorem 1.3.1 (Routh-Hurwitz Criterion)**.** *Given the polynomial*

$$p(\lambda) = \lambda^n + a_1\lambda^{n-1} + ... + a_{n-1}\lambda + a_n$$

with $a_i \in \mathbb{R}$ *for* $i = 1, ..., n$*, define the n Hurwitz's matrices as*

$$H_1 = (a_1), \quad H_2 = \begin{pmatrix} a_1 & 1 \\ a_3 & a_2 \end{pmatrix}, \quad H_3 = \begin{pmatrix} a_1 & 1 & 0 \\ a_3 & a_2 & a_1 \\ a_5 & a_4 & a_3 \end{pmatrix},$$

$$H_n = \begin{pmatrix} a_1 & 1 & 0 & 0 & \cdots & 0 \\ a_3 & a_2 & a_1 & 1 & \cdots & 0 \\ a_5 & a_4 & a_3 & a_2 & \cdots & 0 \\ \vdots & \vdots & \vdots & \vdots & \cdots & \vdots \\ 0 & 0 & 0 & 0 & \cdots & a_n \end{pmatrix},$$

where $a_j = 0$ if $j > n$. All the roots of $p(\lambda)$ are negatives or have negative real part if and only if Hurwitz's determinants are positive, that is

$$\det H_j > 0, \quad j = 1, 2, ..., n.$$

For the proof see [3].
The following example, taken from [2], will be useful in studying one of the treated models in this thesis.

Example 1. If $n = 3$, that is $p(\lambda) = +\lambda^3 + a_1\lambda^2 + a_2\lambda + a_3$, the roots of p are negatives or have negative real part if and only if

$$\det H_1 = a_1 > 0, \ \det H_2 = a_1 a_2 > 0 \ \textit{and} \ \det H_3 = \det \begin{pmatrix} a_1 & 1 & 0 \\ a_3 & a_2 & a_1 \\ 0 & 0 & a_3 \end{pmatrix} = a_1 a_2 a_3 - a_3^2 > 0,$$

that is $a_1 > 0$, $a_2 > 0$, $a_3 > 0$ and $a_1 a_2 > a_3$.

This example will be useful for our purposes in the following sections.

Chapter 2

Cellular Automata

Cellular Automata (CAs from now on) are discrete systems consisting of a big number of simple identical components with local connectivity [25]. Such systems have the ability to perform complex computations with a high degree of efficiency and robustness, as well as to model the behaviour of complicated systems in nature. The potential of this type of discrete model is to be able to describe and predict complex and macroscopic behaviors by defining simple local and repetitive rules [26]. This idea is reflected by the etymology of the Greek word from which the English word automaton (sing. of automata and indicated with CA) derives, which literally means "self-making". For these reasons CAs and related architectures have been studied in biology, mathematics and computer science [27]. They have been used as models of physical and biological phenomena, like biological models formation. CAs have been used as abstract models for studying collective behaviour.

2.1 What is a cellular automaton?

A CA essentially consists of two components:

- the cellular space,
- the transition rule (or CA rule).

The cellular space is a lattice of N cells which can assume a finite number of states, each

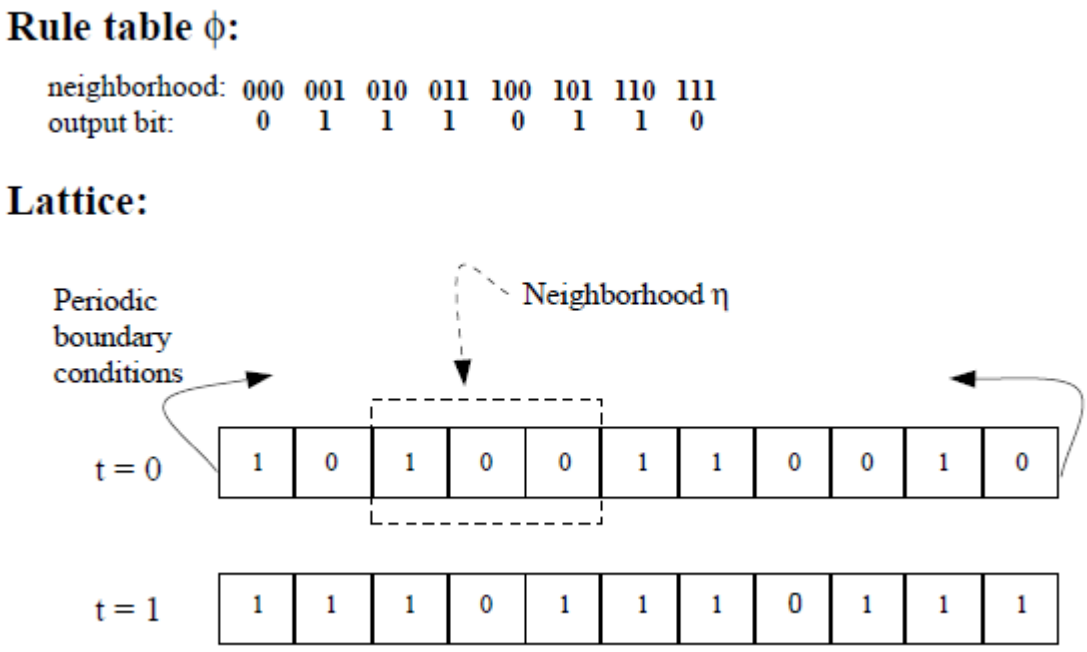

Figure 2.1: Illustration of one dimensional, binary-state, $r = 1$ CA with periodic boundary condition. Image taken from [25].

cell with an identical pattern of local connections to other cells for input and output, also with boundary conditions if the lattice is finite. Let Σ denotes the set of possible states that can be assumed by the cell, and $k = |\Sigma|$ denotes the number of states per cell. Each cell is indicated by an index i and its state at time t is denoted as $s_i^{(t)}$. Obviously $s_i^{(t)} \in \Sigma$. The state $s_i^{(t)}$ of a certain cell i together with the states of the cells to which the cell i is connected is called neighborhood η_i^t of the cell i.
The transistion rule, denoted as $\psi(\eta_i^t)$, allow us to update the state $s_i^{(t)}$ to $s_i^{(t+1)}$ for each cell i, as function of η_i^t.

Let us consider a one-dimensional example taken from [25] and illustrated in Figure 2.1. We can observe that $k = 2$ and $\Sigma = \{0, 1\}$. Here, the neighborhood of each cell consists of itself and its two nearest neighbors and the boundary condition are the following: the leftmost cell is considered to be right neighbor of the rightmost cell, and vice versa. For one dimensional CAs, the size of the neighborhood η_i, omitting t if it is

not needed, is often written as $|\eta_i| = 2r+1$, where r is called the radius of the CA. In our example, $\psi : \Sigma^{2r+1} \longrightarrow \Sigma$. In cases of binary-state CAs, where the number of possible neighborhoods is not too large, the CA rule is often displayed as a rule table, which shows each possible neighborhood together with his output bit, with the updated value for the state of the central cell in the neighborhood. In the specific case of neighborhood marked in Figure 2.1, the corresponding output bit of the sequence 100 is 0, as reported in the center cell of the neighborhood at the next time step.

This kind of CA is one of the simplest form of CA architecture. This basic configuration can be modified in many ways: increasing the number of dimensions, the number of states per cell and the neighborhood size, for example. It is also possible to modify boundary conditions, making the CA rule stochastic rather than deterministic.

Historically, although the original idea of cellular automata is linked to the mathematicians Stanislaw Ulam and John von Neumann already in 1940s, it was in the 1970s that interest in the topic expanded significantly. In particular, in 1970 a sort of milestone in this area was represented by the presentation of a two-dimensional cellular automaton, known as Conway's Game of Life [25].

2.2 The Game of Life

The "Game of Life" was started to invent by John Conway in 1960 and perfected together with Berlekamp and Guy [25]. Game of Life is a binary state automaton, capable of universal computation. The player interacts by setting an initial configuration and observing how it evolves. One peculiar characteristic is that it is a very simple automaton with simple rule which can lead to interesting patterns in the cellular space [23]. It is possible to consider the lattice as two-dimensional and infinite where the neighborhood of each cell is the so-called Moore's one, i.e. composed of a central cell and the eight cells that sourrond it. The automaton starts from a specific configuration [25]. The transition rule, that is the updating from $s_i^{(t)}$ to $s_i^{(t+1)} = \psi(\eta_i^t)$, follows these rules:

- if $s_i^{(t)} = 1$ then $\psi(\eta_i^t) = 1$ if and only if exactly two or three other neighbors are in the 1 state, otherwise $\psi(\eta_i^t) = 0$;

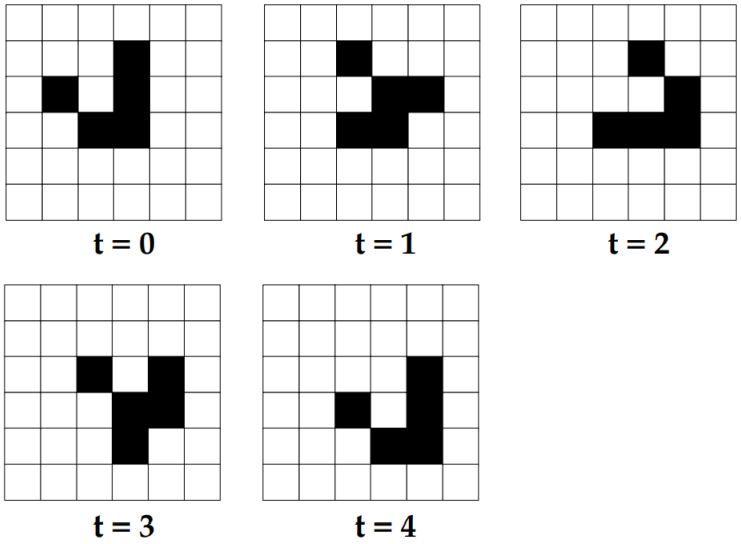

Figure 2.2: Example of the pattern glider in Game of Life. The initial configuration moves one square diagonally every four time steps. Image taken from [25].

- if $s_i^{(t)} = 0$ then $\psi(\eta_i^t) = 1$ if and only if exactly three other neighbors are in the state 1, otherwise $\psi(\eta_i^t) = 0$.

It is amazing as many different kinds of patterns occur during the game. They can be classified according to their behaviour. Common pattern types may include:

- still lifes, that do not change from one generation to the next;
- oscillators, which return to their initial state after a finite number of generations;
- spaceships, which translate themselves across the lattice.

Many other patterns become a combination of these three examples. In Figure 2.2 we display a specific example of spaceship, called glider. More details can be seen in [23] and [25].

Chapter 3

Biomedical applications

3.1 A mathematical model for Alzheimer's disease

In order to understand the development of Alzheimer's disease (AD from now on), a biological description of this dementia is suitable. Alzheimer disease is a very common neurodegenerative disease, firstly described by Alois Alzheimer in 1906 [42], [24]. It is a very serious illness because the etiology, meaning the mechanism and the progression of AD, is still far from understood. Moreover it has a huge social and economic impact, because a person suffering of this pathology becomes seriously not independent.

Being affected by AD means having these manifestations:

- amnesia;
- inability of speaking and understanding verbal messages, called aphasia;
- inability of recognizing people or places , called agnosia;
- inability of completing voluntary movement, called apraxia.

The degenerative process affects cerebral cells and connections. At the beginning, damages to memory and languages manifestations are prevalent. Then the person starts to lost his independence. In the end, he stops to eat, speak and he is forced on the bed.

One of the hallmark of the disease is the accumulation of Amyloidβ (Aβ), a peptide which is found the senile plaques present in diseased brains. It is normally produced

during life by neurons in the central nervous system, through proteolysis of APP, a large trans-membrane protein involved in signal transduction pathways [15]. For unknown and sometimes genetic reasons, malfunctioning neurons present an unbalance between produced and cleared Aβ. This leads to an high concentration of toxic Aβ oligomers. They can form long insoluble chains, known precisely as senile plaques, and can also diffuse through the brain tissue. Their agglomeration can be articulated in several steps: initial seeds, soluble oligomers, protofibrils and insoluble polymers [16],[17].
The connection between Aβ and AD relies on the fact that Aβ plays an important role in the process of celebral damage, called amyloid cascade hypothesis [18], [21]. Soluble Aβ shows multiple neurotoxic effect: it induces a general inflammation that activates the microglia which in turn secretes proinflamamtory cytokines [19] and, at the same time, increases calcium levels [20], which leads to apoptiosis and neuronal death.

3.1.1 The Model

We try now to construct a mathematical model in order to transform biomedical knowledge in some sort of mathematical formulation, which can be studied analytically and numerically. This model is composed by an automaton, which provides to update the state of AD in a specific REV, described below. Indeed, the cerebral region under consideration must be divided in representative elementary volumes, called REV. In each REV we consider a parameter, denoted by a, that takes into account the progression of the disease. Its value is updated according to an ODE system, which models the evolution of Aβ.

For clarity, an index i indicates a polymer length: if $i \leq n$ we are referring to a soluble oligomer, if $i = n$ to an immobile plaque. Aβ peptides merge in the following way. Consider P_j and P_k two soluble oligomers or monomers of length j and k respectively. They merge in a unique polymer, or oligomer, of length $k + j$, denoted as P_{j+k}.

Definition 3.1. $w_i(t)$ denotes the number of soluble amyloid polymers of length i, for $i < n$ contained in a given REV at time t. $W_n(t)$ indicates the total number of immobile particles in the REV. K is a strictly positive constant denoting that two component can merge. If they are very close, they certainly merge very quickly. If they are far away, there are less chances that they merge and the speed of the merging is lower than in the

first case. K^* has the same role of K, but this constant is used to represent the merging between a soluble and immobile polymer.

Now, we can describe the variation of $A\beta$, using the quantities described above. For simplicity, we omit the dependence on t.
The aggregation rate of two soluble oligomers of length i and j, named $R_{i,j}$, is given by the following formula:

$$R_{i,j} = \begin{cases} Kw_iw_j & \text{if} \quad i,j < n, i \neq j \\ \frac{1}{2}Kw_i(w_i - 1) & \text{if} \quad i,j < n, i = j. \end{cases} \tag{3.1}$$

Assuming that two motionless polymers do not merge, the aggregation rate for a soluble and an immobile polymer is as follows:

$$R_{i,n} = K^*w_iW_n \quad i \neq n. \tag{3.2}$$

Observe that, for definition, $R_{i,n} = R_{n,i}$. Since the probability of merging is smaller if one of the two polimers is still, we can consider $K^* < K$.
The evolution of the number of monomers in a given REV is described by the following differential equation:

$$\frac{dw_1}{dt} = -Kw_1 \sum_{j=1}^{n-1} w_j - K^*w_1W_n + \Lambda - M_1w_1 \tag{3.3}$$

where Λ is the production rate of monomers and $M_1 > 0$ is their mortality, that is the clearance due both to the phatologic activity of the microglia and the possible reabsorption by blood vessel [5],[6]. The first, second and fourth term in (3.3) indicate a loss of monomers due respectively to coagulation with oligomers, coagulation with plaques and clearence, while the third term is a gain one.
The evolution of the number of oligomers w_s, with $1 < s < n$, is described by the equation:

$$\frac{dw_s}{dt} = \frac{K}{2} \sum_{i+j=s} w_iw_j - Kw_s \sum_{j=1}^{n-1} w_j - K^*w_sW_n - M_sw_s. \tag{3.4}$$

The coefficient $\frac{K}{2}$ is needed in order to count the number of oligomers once. M_s is a strictly positive constant representing the oligomer's mortality. Finally, the variation of

the number of immobile aggregates is given by:

$$\frac{dW_n}{dt} = \frac{K}{2} \sum_{i+j \geq n; i,j<n} w_i w_j - M_n W_n, \tag{3.5}$$

where M_n is a strictly positive constant representing the plaques mortality.

The next step is to model the progression of AD. For this purpose, we use a Cellular Automata model. We will divide the brain in REVs, described in detail below, where each REV corresponds to a cell. Then, for the CA rule we will establish two formulas: the (3.7), a local formula, and the (3.9), a non-local one. We associate the average degree of malfunctioning of the neurons in each REV with a parameter $a \in [0, 1]$: $a = 0$ means that this portion of the brain is healthy and $a = 1$ corresponds to the complete degeneration. We discuss now the dimension of the REV. It should be large enough to contain a sufficient number of neurons, so that it makes sense to define a quantity a as the average degree of malfunctioning of the neurons contained in the REV. On the other hand, the dimension of the REV must be taken small enough so that the variation of a over the macroscopic scale of the cerebral region could be identifiable. For each REV we assume that a is a non decreasing function of time and its variation is due to two different causes:

- a local effect, caused by the level of toxicity of the Aβ in the REV itself;
- a non-local effect, introduced by degradation of the adjacents REVs.

Concerning the local effect, the current opinion is that, while monomers are innocuous, the neurons's degeneration happens if the concentration of soluble toxic oligomers exceeds a given limit. Denoting with γ_i the toxicity of the oligomers w_i contained in a given REV, we can define for each REV the quantity

$$D = \sum_{i=2}^{n-1} \gamma_i w_i, \tag{3.6}$$

and the degradation occurs when D goes beyond a limit value $D^* > 0$. Since the typical timescale of degradation is much slower than the one of aggregation of Aβ peptides, it is reasonable to consider that there exists $T > 0$ such that a is constant in each of the time intervals $(0, T), (T, 2T), \ldots$, and therefore update a at the times T, $2T$,etc. Typically,

$(0, T)$ can be thought of as a period of 180 days. Based on this considerations we write for the local effect the relation

$$a(t) = a(mT) + \theta[D(mT) - D^*]_+ \quad for \quad mT < t \leq (m+1)T, \tag{3.7}$$

where $[.]_+$ means the positive part and θ is a given positive constant.

To model the non-local effect, we assume that the REVs in which we divide the cerebral region considered are cubes of equal size stacked in such a way that each of them has faces in common with its neighbors. We define the neighborhood of a REV, located in the interior of the region, as composed by 26 cubes that have at least one vertex in common with it, as in Figure 3.1.

Figure 3.1: REV's neighborhood

If we suppose the region embedded in a virtual frame formed by cubes where a is constantly equal to zero, the definition applies to every REV considered. At this point we update the value of a with the following formula:

$$a(t) = a(mT) + \sigma \sum_k [a_k(mT) - a(mT)]_+ \quad for \quad mT < t \leq (m+1)T, \tag{3.8}$$

where the sum ranges over the 26 cubes in the neighborhood of the considered REV and $\sigma > 0$ is a given constant. Now it is possible to update a in our REV by increasing its value if in another REV of the neighborhood a has a bigger value. Equation (3.8) can be easily generalized. For example we could assume that the influence of the neighbors

is different in different directions, i.e. substituting the sum in the RHS by

$$\sum_k \sigma_k [a_k(mT) - a(mT)]_+.$$

Combining (3.7) and (3.8) as follow

$$a(t) = a(mT) + \theta[D(mT) - D^*]_+ + \sigma \sum_k [a_k(mT) - a(mT)]_+ \quad for \quad mT < t \leq (m+1)T, \tag{3.9}$$

we obtain the law by which we update the value of a in each REV of the region at times T, $2T$, etc.

The final step in the construction of this model consists in specifying how the level of degeneration influences the dynamics of the amyloids. The degeneration is twofold:

- brings to the reduction of the number of active neurons,
- increases the production of monomers made by each neuron.

Combining these two effects we can assume that the monomers production rate in the REV per unit time is given by

$$\Lambda = A(1 - a)(1 + \beta a), \tag{3.10}$$

where A is the rate of monomers produced in a healthy REV and $\beta > 1$ is a given constant. It is known that, during the progression of AD, the maximum production of the amyloid protein can be 4-6 times larger than in a healthy brain [7]. Then, accordingly to [43], we will choose $\beta = 15$.

3.1.2 A specific example

To test the model, we consider the following simplified situation: the total population of amyloids can be divided into 3 subpopulations: monomers, toxic oligomers and immobile aggregates, called also polymers and plaques. We rescale w_i for $i = 1, 2, 3$ by a constant N, described in the following, in order to define:

$$X(t) = \frac{w_1(t)}{N}, \quad Y(t) = \frac{w_2(t)}{N}, \quad Z(t) = \frac{w_3(t)}{N}.$$

As [8] explains, the mass of a monomer is about $8 \cdot 10^{-12}$ nanograms. We choose $N = 10^{11}$, corresponding to the order of magnitude of the number of monomers in a nanogram. So X represents, in order of magnitude, the mass of monomers in nanograms in the considered REV. For the evolution of the amyloids we choose one day as unit time.
Setting $k = K \times N$, $k^* = K^* \times N$ and $\lambda = \frac{\Lambda}{N}$ and omitting the dependence on t, the differential equations (3.3), (3.4), (3.5) take the form:

$$\begin{cases} X' = -kX^2 - kXY - k^*XZ - M_1X + \lambda & (A) \\ Y' = \frac{1}{2}kX^2 - kXY - kY^2 - k^*YZ - M_2Y & (B) \\ Z' = \frac{1}{2}kY^2 + kXY - M_3Z & (C) \end{cases} \tag{3.11}$$

The rescaled expression for λ is, using (3.10), $\lambda = \lambda_0(1-a)(1+\beta a)$ where $\lambda_0 = \frac{A}{N}$. The choice $\lambda_0 = 2$ corresponds to a daily monomer production of 2 nanograms in each REV and 1000 nanograms in a healthy brain. According to the literature [14], this choice seems reasonable. We now choose the remaining constants in (3.11). Assuming that the daily clearance amounts to 1%, we take $M_i = 10^{-2}$ for $i = 1, 2, 3$, [14]. Althought in the literature there are various attempts to give explicit formulas for k and k^* [9], [10], [11], this last choice remains arbitrary and in all our AD simulations we consider $k = 10^{-4}$ and $k^* = 5 \cdot 10^{-6}$, [14]. In table 3.1 we summarize all the choices made for the parameters. These choices will never change in all our tests.

parameter	value
β	15
λ_0	2
M_1	10^{-2}
M_2	10^{-2}
M_3	10^{-2}
k	10^{-4}
k^*	$5 \cdot 10^{-6}$

Table 3.1: Summarizin of parameter's choices.

In this context we stress that our example is rather conceptual and speculative, and mainly aimed to illustrate the potentiality of the model.

We are now interested in studying the system (3.11), its solutions and its equilibrium values.

3.1.3 Global existence of solutions

We consider the system (3.11) with positive initial data $X(0) := X_0$, $Y(0) := Y_0$, $Z(0) := Z_0 > 0$. This system has a global positive solution, as shown below. The local solutions X, Y, Z of (3.11), defined on $[0, T]$, exist for the Peano-Picard theorem and are $C^1([0, T])$, since the first derivatives of X, Y, Z are polynomials.

We begin by showing that the local solutions corresponding to strictly positive initial data are strictly positive.

Theorem 3.1.1. *If X_0, Y_0, Z_0 are positive, then $X(t) > 0, Y(t) > 0$ and $Z(t) > 0 \quad \forall t \in [0, T]$.*

Proof. Consider $X(t)$. Suppose for the sake of argument $X(t) \leq 0$, for some $t \in \mathbb{R}^+$. Let t^* be the first value such that $X(t^*) = 0$ which certainly exists for the zero's theorem, since $X(0) = X_0 > 0$. Substituting $X(t^*)$ in (A) we obtain $X'(t^*) = \lambda > 0$, which means X has positive tangent in t^*. This is absurd because for $t < t^*$ we have $X(t) > 0$ and for $t > t^*$ we have $X(t) \leq 0$.
In the same way we show the statement for Y. Consider t^{**} be the first value such that $Y(t^{**}) = 0$. Substituting in (B) we obtain $Y' = \frac{1}{2}kX^2(t^{**}) > 0$, meaning that Y has a positive tangent t^{**}. This is absurd for the reasons as above.
The proof for Z is the analogous, choosing a value t^{***}. □

So X, Y, Z are strictly positive on $[0, T]$. We prove that they are limited on $[0, T]$ in two different ways. Then by applying the Theorem 3.1.4, we can extend the solutions of our system to all $t > T$

Theorem 3.1.2. *The solutions X, Y, Z are limited on $[0, T]$.*

Proof. For $X(t)$, from (A) and knowing that X, Y, Z are positive, we obtain $X'(t) < \lambda$. Then, by the fundamental theorem of calculus we have

$$X(t) = X_0 + \int_0^T X'(s)ds \leq X_0 + \lambda T := X_0 + c_1 T,$$

where c_1 is a constant value. Similarly for $Y(t)$. From (B) we have $Y'(t) < \frac{1}{2}k(X_0+\lambda T)^2$. Therefore

$$Y(t) = Y_0 + \int_0^T Y'(s)ds \leq Y_0 + \int_0^T (\frac{1}{2}kX_0^2 + \frac{1}{2}k\lambda^2T^2 + kX_0\lambda T)ds =$$

$$= Y_0 + (\frac{1}{2}kX_0^2 + \frac{1}{2}k\lambda^2T^2 + kX_0\lambda T)T := Y_0 + c_2T,$$

where c_2 is a constant value. Likewise for Z we can estimate this function with a constant c_3 and write

$$Z(t) \leq Z_0 + c_3T$$

□

Another way to prove that X, Y, Z are limited is the following:

Theorem 3.1.3. *The following inequalities holds:*
$X' \leq -kX^2 + \lambda - k^*XZ \Rightarrow X(t) \leq \alpha := \max\{X(0), \sqrt{\frac{\lambda}{k}}\}$
$Y' \leq k\alpha^2 - kY^2 - k^*YZ \Rightarrow Y(t) \leq \beta := \max\{Y(0), \alpha\}$
$Z' \leq \frac{1}{2}k\beta^2 + k\alpha\beta - M_3 \Rightarrow Z(t)$ *is also limited.*

Proof. We prove the statement only for X.
Define $\alpha := max\{X(0), \sqrt{\frac{\lambda}{k}}\}$. We can consider two cases:
1. $X_0 \geq \sqrt{\frac{\lambda}{k}}$;
2. $X_0 < \sqrt{\frac{\lambda}{k}}$.
1. If $X_0 \geq \sqrt{\frac{\lambda}{k}}$ then $\alpha = X(0)$. Using (A) and here substituting $\sqrt{\frac{\lambda}{k}}$ we obtain $X'(0) \leq -k\sqrt{\frac{\lambda}{k}} + \lambda - k^*X(0)Z(0) < 0$. Then, being $X'(0) < 0$, we have that in a right neighborhood of 0 X decreases. At this point there are two possible cases:
1a. $X(t) < \alpha \quad \forall t \in [0, +\infty] \Rightarrow$ we obtain the inequality we wanted.
1b. $\exists t^* > 0$ such that $X(t^*) = \alpha(\geq \sqrt{\frac{\lambda}{k}})$. But then, the inequality

$$X'(t^*) \leq -kX^2(t^*) + \lambda - k^*X(t^*)Z(t^*) \leq -k^*X(t^*)Z(t^*) < 0$$

implies that in a right neighborhood of t^* must be $X(t) > \alpha$, that is absurd.
2. $X_0 < \sqrt{\frac{\lambda}{k}}$. Since in this case $\alpha = \sqrt{\frac{\lambda}{k}}$, for a well known theorem, [44], $X(t)$ takes smaller values than α. Then there exists $\bar{t}$ such that $X(t) < \alpha$ on $[0, \bar{t}]$. Consider now

$t^* = \sup\{t > 0; \quad X(s) < \alpha \quad on \quad [0, \bar{t}]\}$, that is t^* is the first t such that $X(t)$ reaches α. Then, for the very definition of sup, $X(t^*) = \alpha$. Thinking as above

$$X'(t^*) \leq -k\alpha^2 + \lambda - k^* X(t^*) Z(t^*) < 0$$

and this implies that X decreases in t^*, that is $X(t) \geq X(t^*) = \alpha$ for $t \in [t^* - \delta, t^*]$. This is absurd for the very definition of t^*. So $t^* = +\infty$ □

We now apply the Theorem below to obtain global existence of the solutions.

Theorem 3.1.4. *Suppose $f : I \times \mathbb{R}^n \longrightarrow \mathbb{R}^n$. If for every closed and limited interval $I' \subset I$ there exist constants V_1, V_2 such that $\|f(t,x)\| \leq V_1 + V_2\|x\|$, then every maximal solution of the system $\dot{x} = f(x)$ is defined on all I.*

For the proof see [1].

We have therefore that the solutions exist $\forall t > T$, that is their domain is $\mathbb{R}^+ \cup \{0\}$.

3.1.4 Dependence on initial data

After having showed positivity, boundedness and extensibility of the solutions, we analyze their dependence on initial data. First we solve this system using $a = 0$ and then using $a = 0.02$. In each case, three possible initial configurations are considered:

- $X_0 = 10$, $Y_0 = 1$, $Z_0 = 1$;
- $X_0 = 15$, $Y_0 = 1$, $Z_0 = 1$;
- $X_0 = 20$, $Y_0 = 1$, $Z_0 = 1$.

In Figure 3.2 we can see that in each of the two cases, starting from different configurations, the same equilibrium point is reached and it does not depend on the initial data. This results is reasonable, because if we study the equilibrium points, as we will do in the following subsection, we will notice that for fixed parameters, including a fixed a, there is a unique equilibrium point that does not depend on the initial data. Observe that varying the initial mass of monomers reflects exactly what just explained for AD, where the illness is originated by an excess of monomers of Aβ.

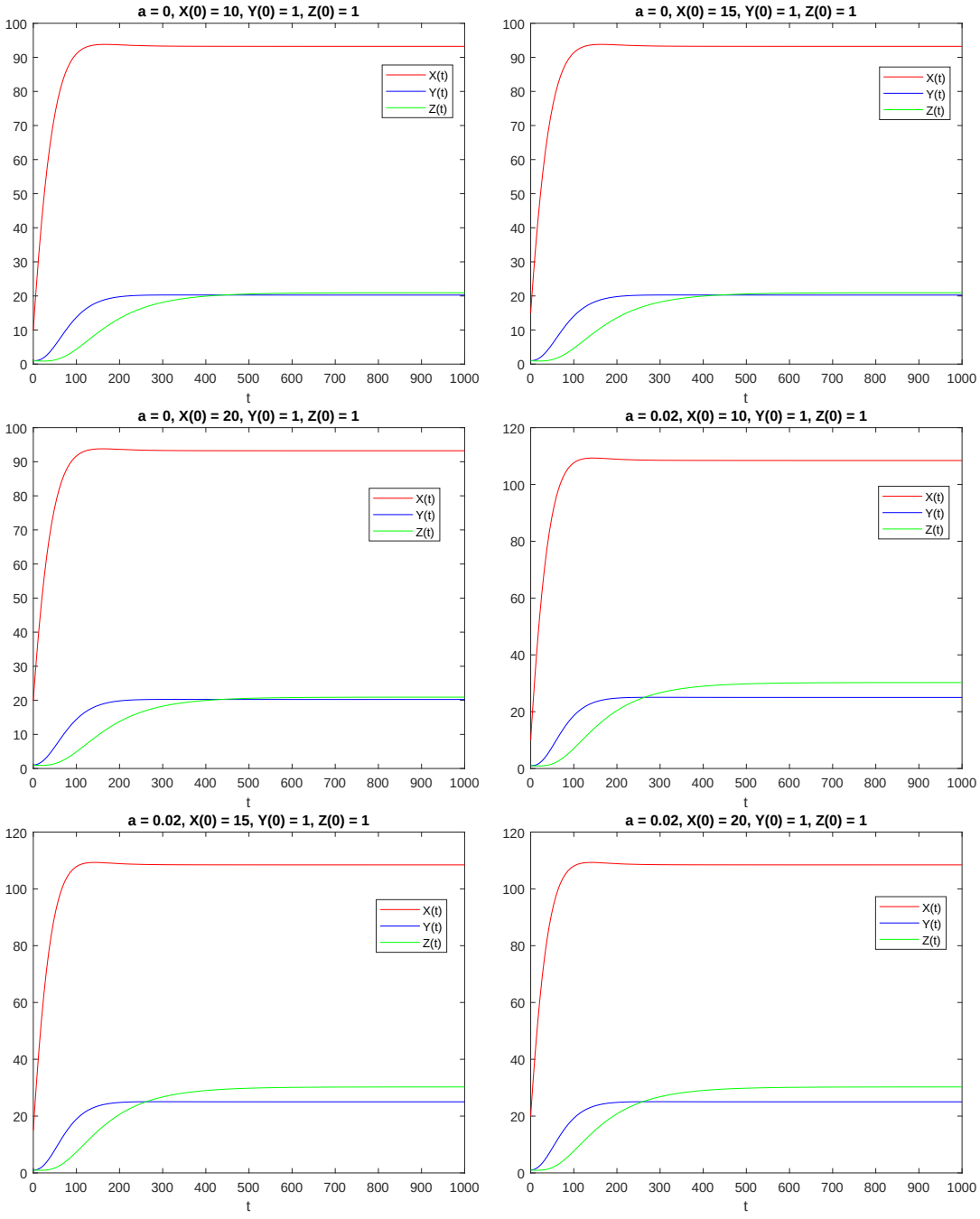

Figure 3.2: Graphs with different initial data in two possible AD situations: $a = 0$ and $a = 0.02$.

3.1.5 Equilibrium solutions

Consider now the equilibrium solutions of the system (3.11), that is the solutions of the algebraic system

$$\begin{cases} 0 = -kX^2 - kXY - k^*XZ - M_1X + \lambda & (A') \\ 0 = \frac{1}{2}kX^2 - kXY - kY^2 - k^*YZ - M_2Y & (B') \\ 0 = \frac{1}{2}kY^2 + kXY - M_3Z. & (C') \end{cases} \tag{3.12}$$

We shall prove that the system (3.11) has an equilibium solution

$$X \equiv X_0 > 0, \quad Y \equiv Y_0 > 0, \quad Z \equiv Z_0 > 0.$$

and that this solution is unique. First we study the existence of equilibrium solutions. Solutions of (3.12) satisfy

$$Z = \frac{k}{2M_3}Y^2 + \frac{k}{M_3}XY$$

and

$$\begin{cases} -kX^2 - kXY - k^*X(\frac{k}{2M_3}Y^2 + \frac{k}{M_3}XY) - M_1X + \lambda = 0 \\ \frac{1}{2}kX^2 - kXY - kY^2 - k^*Y(\frac{k}{2M_3}Y^2 + \frac{k}{M_3}XY) - M_2Y = 0, \end{cases} \tag{3.13}$$

that is a system of two quadratic equations in X:

$$\begin{cases} (1 + \frac{k^*}{M_3})X^2 + (Y + \frac{k^*}{2M_3}Y^2 + \frac{M_1}{k})X - \frac{\lambda}{k} = 0 \\ X^2 - 2(Y + \frac{k^*}{M_3}Y^2)X - 2Y^2 - \frac{k^*}{M_3}Y^3 - \frac{2M_2}{k}Y = 0. \end{cases} \tag{3.14}$$

The positive solutions of the second degree equations are:

$$X = X_1(Y) = \frac{-(Y + \frac{k^*}{2M_3}Y^2 + \frac{M_1}{k}) + \sqrt{(Y + \frac{k^*}{2M_3}Y^2 + \frac{M_1}{k})^2 + \frac{4\lambda}{k}(1 + \frac{k^*}{M_3}Y)}}{2(1 + \frac{k^*}{M_3}Y)}$$

and

$$X = X_2(Y) = Y + \frac{k^*}{M_3}Y^2 + \sqrt{(Y + \frac{k^*}{M_3}Y^2)^2 + 2Y^2 + \frac{k^*}{M_3}Y^3 + \frac{2M_2}{k}Y}.$$

Observe that X_1 and X_2 have the following properties:

- $X_2(Y)$ is strictly decreasing,

- $X_2(0) = 0$
- $X_2(\infty) = \infty$
- $X_1(0) = -\frac{M_1}{2k} + \frac{1}{2}\sqrt{(\frac{M_1}{k})^2 + \frac{4\lambda}{k}} > 0$
- $X_1(Y) = \frac{Y+\frac{k^*}{2M_3}Y^2+\frac{M_1}{k}}{2(1+\frac{k^*}{M_3}Y)}(-1+\sqrt{1+\frac{\frac{4\lambda}{k}(1+\frac{k^*}{M_3}Y)}{(Y+\frac{k^*}{2M_3}Y^2+\frac{M_1}{k})^2}}) = \frac{Y+\frac{k^*}{2M_3}Y^2+\frac{M_1}{k}}{2(1+\frac{k^*}{M_3}Y)}(\frac{\frac{4\lambda}{k}(1+\frac{k^*}{M_3}Y)}{2(Y+\frac{k^*}{2M_3}Y^2+\frac{M_1}{k})^2})(1+o(1)) \to 0$ as $Y \to \infty$.

Therefore the curves $X = X_1(Y)$ and $X = X_2(Y)$ have at least one intersection point (X_0, Y_0), which corresponds to an equilibrium solution (X_0, Y_0, Z_0), where $Z_0 = \frac{k}{2M_3}Y_0^2 + \frac{k}{M_3}X_0Y_0$.
Now we show the uniqueness of the equilibrium solution.
Let us observe preliminarily that a solution (X_0, Y_0, Z_0) of the system (3.12) satisfies $X_0 > 0$, $Y_0 > 0$ and $Z_0 > 0$ (see Theorem 3.1.1). The last equation shows that

$$M_3Z = \frac{1}{2}kY^2 + kXY. \tag{3.15}$$

Substituting in the first equation of (3.12) we have:

$$\begin{cases} 0 = -kX^2 - kXY - \frac{k^*}{M_3}X(\frac{1}{2}kY^2 + kXY) - M_1X + \lambda & (A'') \\ 0 = \frac{1}{2}kX^2 - kXY - kY^2 - \frac{k^*}{M_3}Y(\frac{1}{2}kY^2 + kXY) - M_2Y & (B'') \\ 0 = \frac{1}{2}kY^2 + kXY - M_3Z. & (C'') \end{cases} \tag{3.16}$$

Multiplying (A'') by $-Y$ and (B'') by X we obtain:

$$\begin{cases} 0 = -kX^2Y - kXY^2 + \frac{k^*}{M_3}XY(\frac{1}{2}kY^2 + kXY) + M_1XY - \lambda Y & (A'') \\ 0 = \frac{1}{2}kX^3 - kX^2Y - kXY^2 - \frac{k^*}{M_3}XY(\frac{1}{2}kY^2 + kXY) - M_2YX & (B'') \\ 0 = \frac{1}{2}kY^2 + kXY - M_3Z. & (C'') \end{cases} \tag{3.17}$$

Summing (A'') with (B'') in (3.17) we have

$$\lambda Y = kX^2Y + kXY^2 + \frac{kk^*}{2M_3}X^2Y^2 + M_1XY +$$

$$+\frac{1}{2}kX^3 - kX^2Y - kXY^2 - \frac{kk^*}{2M_3}XY^3 - \frac{kk^*}{M_3}X^2Y^2 - M_2YX,$$

and

$$Y(\lambda + (M_2 - M_1)X) = \frac{k}{2}X^3.$$

Since, as we just showed, $X > 0$, we have $\frac{k}{2}X^3 > 0$ and, by $Y > 0$ we obtain $\lambda + (M_2 - M_1)X > 0$. Let us consider now the function

$$F(X) = \frac{\frac{k}{2}X^3}{\lambda + (M_2 - M_1)X}$$

defined on the set

$$I = \{X > 0, \lambda + (M_2 - M_1)X > 0\}.$$

Calculating the derivative of F, we have

$$F'(X) = \frac{\frac{3k}{2}X^2(\lambda + (M_2 - M_1)X) - \frac{k}{2}X^3(M_2 - M_1)}{(\lambda + (M_2 - M_1)X)^2}$$

and if the numerator of F' is positive, F' is positive on the same set. So, we notice that

$$\frac{3k}{2}X^2(\lambda + (M_2 - M_1)X) - \frac{k}{2}X^3(M_2 - M_1) = kX^3(M_2 - M_1) + \frac{3k\lambda}{2}X^2 =$$

$$= kX^2(X(M_2 - M_1) + \frac{3\lambda}{2}) > \frac{\lambda}{2} > 0$$

By contradiction, if (X_0, Y_0, Z_0) and (X_1, Y_1, Z_1) are two different solutions of (3.12) with $0 < X_0 < X_1$, we have $0 < Y_0 < Y_1$. Then the first equation of (3.16) gives:

$$\lambda = kX_0^2 + kX_0Y_0 + \frac{k^*}{M_3}X_0(\frac{1}{2}kY_0^2 + kX_0Y_0) + M_1X_0 <$$

$$< kX_1^2 + kX_1Y_1 + \frac{k^*}{M_3}X_1(\frac{1}{2}kY_1^2 + kX_1Y_1) + M_1X_1 = \lambda,$$

bringing to a contradition. Now, in Figure 3.3,we display the equilibrium points in two possible configurations of AD.

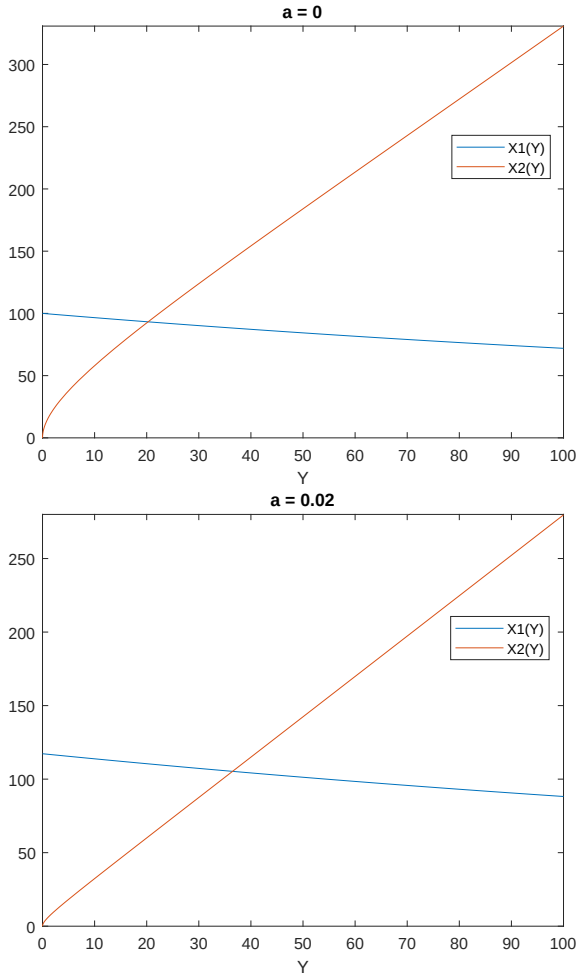

Figure 3.3: Intersection of $X_1(Y)$ and $X_2(Y)$ in order to study equilibrium solutions for different values of a.

3.1.6 Stability of equilibrium solutions

As we discussed in Chapter 1, equilibrium points can be asymptotically stable, stable or unstable. Applying this theory, it is possible to study the stability of the equilibrium solution of (3.11). For our analysis, we assume $M_1 = M_2 = M_3 = M$ for simplicity. Our system is nonlinear, so we need to linearize it around the equilibrium solution by

calculating the jacobian matrix. The matrix is the following:

$$J = \begin{pmatrix} -2kX - kY - k^*Z - M & -kX & -k^*X \\ kX - kY & -kX - 2kY - k^*Z - M & -k^*Y \\ kY & kX + kY & -M \end{pmatrix},$$

To study the stability of the linearized system $x' = Jx$ corresponds to study the local stability of (3.11). In order to use what we explained in Chapter 1, it is necessary to calculate the characteristic polynomial of J and to establish if it is a Hurwitz polynomial. The characteristic polynomial for J is:

$$P(u) = -u^3 - au^2 - bu - c,$$

where

- $a = -3M - 3kX - 3kY - 2k^*Z$;
- $b = -3M^2 - 6kMX - 3k^2X^2 - 6kMY - 4k^2XY - 2kk^*XY - 2k^2Y^2 - kk^*Y^2 - 4k^*MZ - 3kk^*XZ - 3kk^*YZ - k^{*2}Z^2$;
- $c = -M^3 - 3kM^2X - 3k^2MX^2 - k^2k^*X^3 - 3kM^2Y - 4k^2MXY - 2kk^*MXY - 3k^2k^*X^2Y - 2k^2MY^2 - kk^*MY^2 - 3k^2k^*XY^2 - k^2k^*Y^3 - 2k^*M^2Z - 3kk^*MXZ - 3kk^*MYZ - 2kk^{*2}XYZ - kk^*Y^2Z - k^*MZ^2$.

Using the notations of Chapter 1, since $a = -a_1$, $b = -a_2$ and $c = -a_3$, we have tro prove that $a * b + c > 0$. Using Mathematica software, we have that this condition is verified if

$$k^* > 0, \quad k \geq \frac{k^*}{9}, \quad M > 0, \quad X > 0, \quad Y > 0, \quad Z > 0,$$

(see section 4.3). This requirements are verified by our proofs (positivity of solutions) and the assumptions on the parameters. So the equilibrium point is asymptotically stable. This result reflects the behaviour of the solution, for a fixed a, since they tend towards a fixed value, as seen in Figure 3.2.

3.1.7 Progression of the disease

After having deeply analyzed the system (3.11), we study the development of AD with local and non-local influence, in the two-dimensional case. In this context we consider each REV as two-dimensional, so it corresponds to a face of the cube in Figure 3.1. Then we display the solution of (3.11), depending on the worsening of the disease.

Remember the system (3.11) in exam:

$$\begin{cases} X' = -kX^2 - kXY - k^*XZ - M_1X + \lambda \\ Y' = \frac{1}{2}kX^2 - kXY - kY^2 - k^*YZ - M_2Y \\ Z' = \frac{1}{2}kY^2 + kXY - M_3Z \end{cases}$$

where X, Y, Z represent respectively the quantity of monomers, oligomers and plaques. The only toxic component in our model is given by Y and for these simulations we choose $D^* = Y^* = 22$. The remaining parameter γ_2 from (3.6), is setted equal to 1. As already pointed out, the local progression of AD is governed by (3.7), while the non-local one is driven by (3.9). As said in the second section of this chapter, the a parameter is updated every 180 days. In each case we display the grids which represent a brain divided in 20×20 cells representing the REVs.

We examine first the local case. Applying formula (3.7), it is easy to monitor the development of AD in a specific REV, here the one of coordinates $(6, 6)$, as in Figure 3.4. The graph represents exactly our expectation: a is non-decreasing function of time and it tends towards 1. Then, we can see the development of AD in the 20×20 grids represented in Figure 3.5. The other parameters are chosen as usual.

We study now the non-local effect on a. The grids presented in Figure 3.6 show us how the AD expands. Starting from the $(6, 6)$ REV, the AD progresses and enlarges its area. That area looks like a circle because no direction is preferred for the diffusion of the disease. The grid at $t = 0$ is not represented because it is the same as above, represented in Figure 3.5.

Concerning the non-local effect, it is possible to analyze the behavior of a in different REVs. Figure 3.7 shows the graphs of a in three REVs. The values of the curves reflect exactly what found in the grids. The $(18, 18)$ REV, far from the $(6, 6)$ one, doesn't became ill. The $(8, 6)$ REV, which is close to the $(6, 6)$ one, becomes ill very quickly and

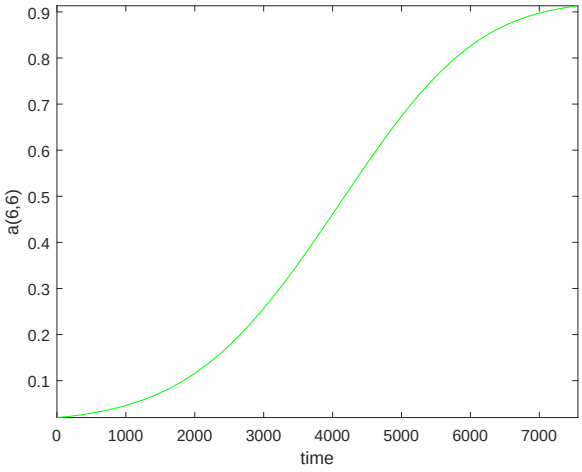

Figure 3.4: Development of AD with $a(0) = 0.02$, using the local formula (3.7).

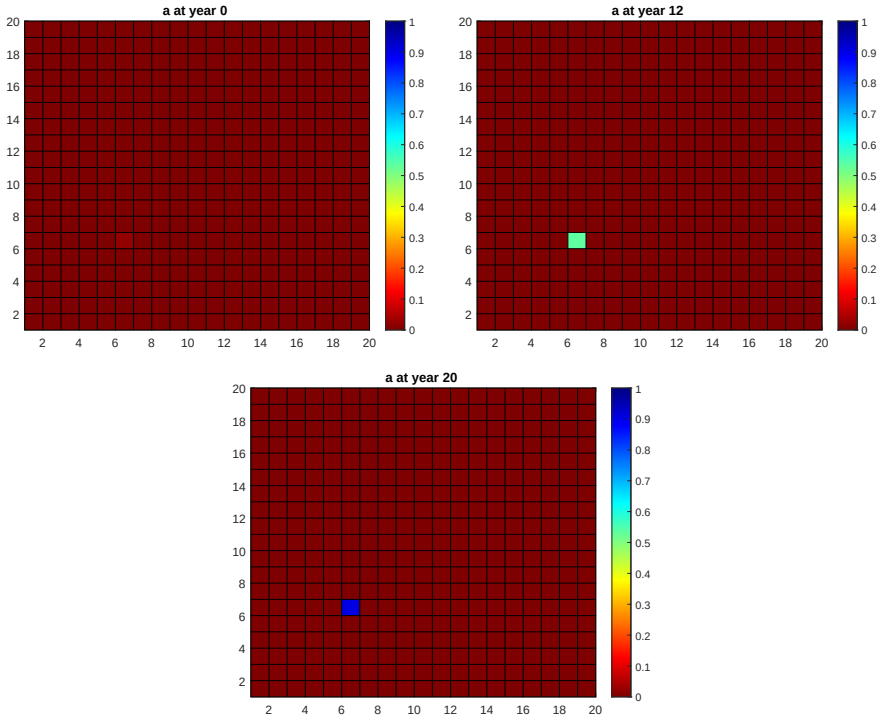

Figure 3.5: Images representing the progression of AD with local effect on a starting from $a(0) = 0.02$ in the $(6, 6)$ REV.

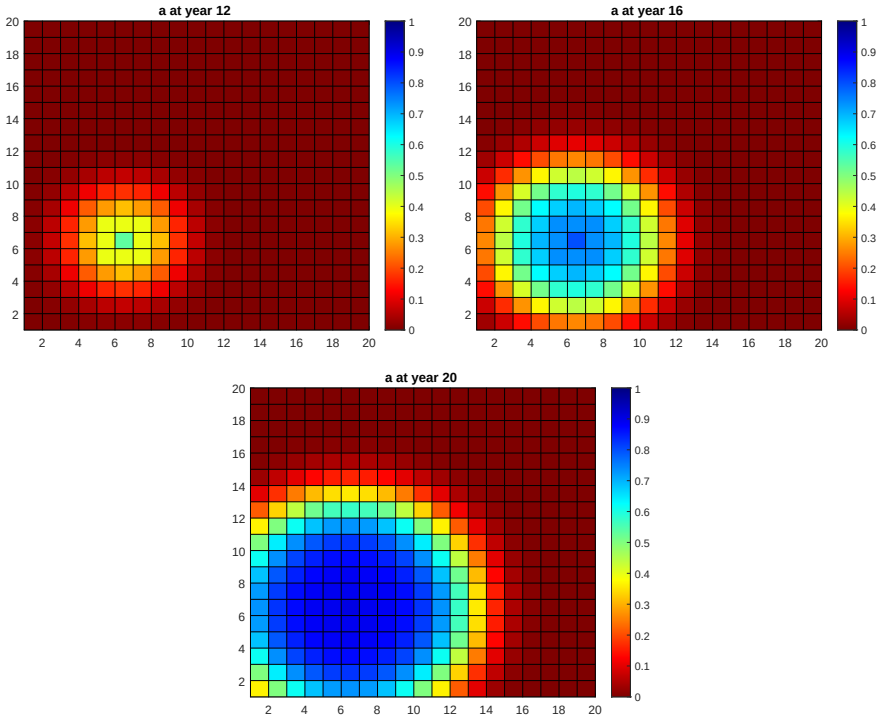

Figure 3.6: Images representing the progression of AD with non-local effect on a, starting from $a(0) = 0.02$.

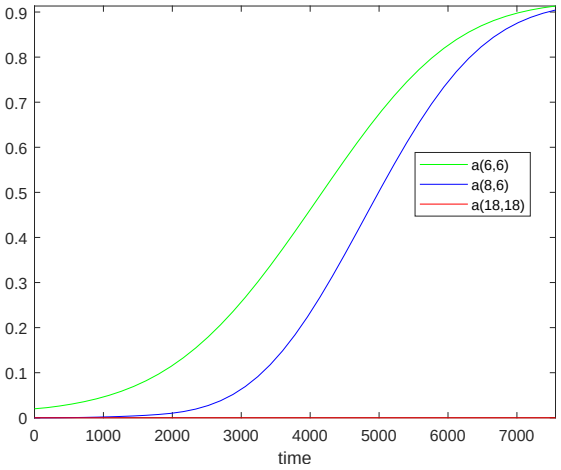

Figure 3.7: Development of AD in three different REVs calculated with (3.9).

its values became more and more close to the $(6, 6)$ ones.

Using the non-local approach, it is possible to calculate the solution X, Y, Z influenced by the progression of the disease. This means to calculate the solution in a range of 180 days, update a with the (3.9) formula and to insert this value for the calculus in the following 180 days, and so on. This type of solution is showed in Figure 3.8. We see here that the solutions do not approach an equilibrium value. This is an interesting effect which should be possibily studied also analitically. The choice of using (3.9) for studying

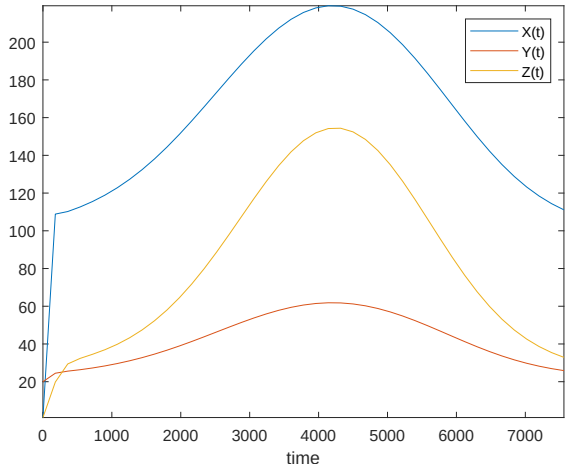

Figure 3.8: Solution X, Y, Z for the REV $(6, 6)$ calculated with non-local effect formula (3.9) for updating a.

the development of AD with an evolving value for a can be replaced with a different updating scheme for a, divided in two steps: first a local updating with (3.7) and then a global updating using (3.8). We will investigate this possibility in the future.

3.2 Mathematical models for tumours with cancer stem cells

In the last few years several articles has been devoted to the construction, discussion and analysis of mathematical models describing the growth of tumors in presence of cancer stem cells (CSC from now on) [45], [46], [47]. CSC has been founded in many cancers, as well as in sarcomas and leukemia. One of the characteristics of tumors with CSC is the so-called tumor-growth paradox, that consist in the fact that tumors with a larger death rate for ordinary (non-stem) cancer cells (CC from now on) might grow bigger than tumors with a lower death rate for the same class of cells. Of course, since the death rate is influenced by medical treatment, understanding the reasons behind this paradox can be relevant in the control and therapy of the tumors. Concerning what we will explain in this section, we have to underline that it is not intended to give quantitative prevision of the progression of cancers, nor to include all possible factors and aspects that influence their growth. It is rather oriented to offer an idea of the phenomenon and to isolate the mechanisms that seem to be crucial for the essential properties of the evolution of tumors in presence of CSC. In the following models, one based on ODE and the other on Cellular Automata, some drastic simplifications are introduced in order to provide mathematical schemes showing solutions that can be investigated and simulated [28].

3.2.1 Hypothesis

The models we will illustrate contain two basic simplifications. The first simplification consists in supposing that the population of tumor's cells is made of two subpopulations: cancer stem cells (CSC) and ordinary non-stem cells (CC). All the cells in each subpopulation have the same properties. The second approximation is that cells have age-independent replicative potential and mortality. In order to be more specific, for CC there is a fixed probability of generating new CC or of undergoing apoptosis, while CSC are considered immortal and capable of generating new CSC or CC, with a fixed proportion between the two probabilities. Even with these simplifications, our models are appropriate to describe the tumor paradox adequately. An important effect

that is considered is the 'crowding effect'. This means that mitosis is supposed to be inhibited when the density of cells in a neighborhood of the would-be mother cell exceeds a limit value. If the model would not include the crowding effect, it would not be able to reproduce the tumor growth paradox [13]. In what follows we do not take into account explicitly the movement of cells provoked by the mutual pushing effect of mitosis.

3.2.2 The ODE model

Let us define $u(t_k)$ the number of the lattice sites occupied by CSC at time t_k divided by the total number of sites. Similarly, $v(t_k)$ represents the fraction of CC at time t_k. In this context we formally consider that the neighborhood of each cell is the entire grid, so the fraction of the vacant sites where a new cell can appear is $1 - u(t_k) - v(t_k)$ at time t_k. Moreover, our discussion considers tumors with cancer stem cells and thus we assume that $u(0) > 0$.

Then, if we look for a continuous evolution system reflecting our hypothesis, we can consider to the following pair of ordinary differential equations:

$$\begin{cases} \frac{du}{dt} = \rho_u \delta u(1-u-v) \\ \frac{dv}{dt} = \rho_u(1-\delta)u(1-u-v) + \rho_v v(1-u-v) - \mu v \end{cases} \tag{3.18}$$

where:

- ρ_u is the replication rate for CSC;
- ρ_v is the replication rate for CC;
- δ is the rate for which a CSC generates a CSC;
- $1-\delta$ is the rate for which a CSC generates a CC ;
- μ is the rate of undergoing apoptosis of a CC;

(see [28]). The first term in both equations (3.18) represents the gain in new CSC and CC from CSC, the second term in the second equation of (3.18) represents the gain in new CC from CC and finally the third term in $\frac{dv}{dt}$ is the loss in CC due to CC apoptosis.

The system (3.18) has a unique steady state $u = 1$ and $v = 0$ which is the only global attractor in the invariant set

$$\Sigma = \{(u, v) : \quad u > 0, \quad v \geq 0, \quad u + v \leq 1\},$$

(see [13]). This corresponds to a situation in which, independently of the proliferation and death rate of the two sub-populations, the tumor occupies the whole available space and consists of stem cells only.

Normalizing respect to time, we have a system with three parameters:

- δ,
- $\rho = \frac{\rho_u}{\rho_v}$,
- $\mu^* = \frac{\mu}{\rho_u}$.

To simplify the notation we will write μ instead of μ^*. The system (3.18) becames:

$$\begin{cases} \dot{u} = \delta u(1 - u - v) \\ \dot{v} = (1 - \delta)u(1 - u - v) + \rho v(1 - u - v) - \mu v. \end{cases} \tag{3.19}$$

The solution of the system (3.19) is reported in Figure 3.9 under the following setup of parameters: $\rho = 0.5$, $\delta = 0.2$ and $\mu = 1.5$.

As we see in the following simulation, this model is able to reproduce the tumor growth paradox. We fix the parameters setup, as can be seen in the caption of Figure 3.10, but we vary the mortality μ. Figure 3.10 shows the expected paradoxical phenomenon: cells with bigger mortality (green, $\mu = 1.5$) expand faster than ones with lower mortality (yellow, $\mu = 0.5$). This provokes, after a certain time, a bigger tumor for $\mu = 1.5$ than for $\mu = 0.5$.

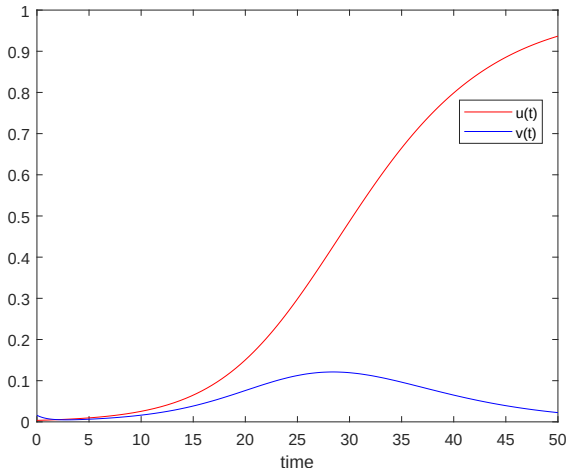

Figure 3.9: Solution of (3.19) with $\rho = 0.5$, $\delta = 0.2$, $\mu = 1.5$.

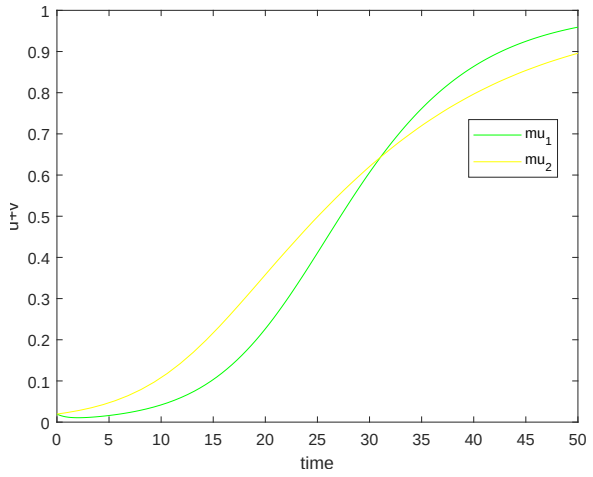

Figure 3.10: Sum of u and v of (3.19) with $\rho = 0.5$, $\delta = 0.2$, $\mu = 1.5$ (green) and $\rho = 0.5$, $\delta = 0.2$, $\mu = 0.5$ (yellow).

3.2.3 The Cellular Automata model

It is possible to simulate tumor growth using Cellular Automata. This is a very interesting approach because we can see the tumor growth and evolution at different times. In this section we provide 2-dimensional [28] and 3-dimensional simulations [29].

First, let us consider the 2d case. Imagine cells as living in a square lattice. It is possible to establish probabilistic rules for their motion, replication or death. When

we run a simulation, the individual behavior of each cell contributes to the evolution of the collective behaviour. According to the observation on the crowding effect, we assume that cells can proliferate only if in their neighborhood some cells are vacant. It is also assumed that dead cells leave immediately empty the site they occupied. Different definitions of neighborhood are possible: for the 2-D lattice Von Neumann's or Moore's neighborhood can be used [25]; while in the 3d simulation the neighborhood of each cell corresponds to a face of the cube represented in Figure 3.1. Moreover, each site in the lattice grid can be in one of three different states:

- empty sites (white),
- CSC occupied sites (black),
- CC occupied sites (red).

Starting from a given situation at time t_k each CC (red) has a probability μ of becoming white. Then, the surviving cells have a probability ρ to be replicant. But, in this case, mitosis is only possible if there are white sites in the chosen neighbourhood; if this situation occurs a daughter CC appears and one of these white sites becomes red. The situation with CSC has two differences:

- $\mu = 0$ (CSC are immortal),
- if mitosis occurs a daughter CSC appears with probability δ, a CC appears with probability $1 - \delta$.

The replication probability ρ can be different for the two types of cells: we denote ρ_u for CSC and ρ_v for CC. We also assume that the replication potential does not depend on the age. In our case the simulation stops before the growing tumor reaches the boundary of the grid, so it is not necessary to specify boundary conditions. In Figure 3.11 we can see the tumor growth in different time steps, for the 2d case.

Let us examine now the three-dimensional case. In this case, our neighborhood is a 3×3 cube within 26 little cubes, as the one in Figure 3.1. So, each cell can interact with another cell which has in common a side or an edge. For CSC, we assume that the

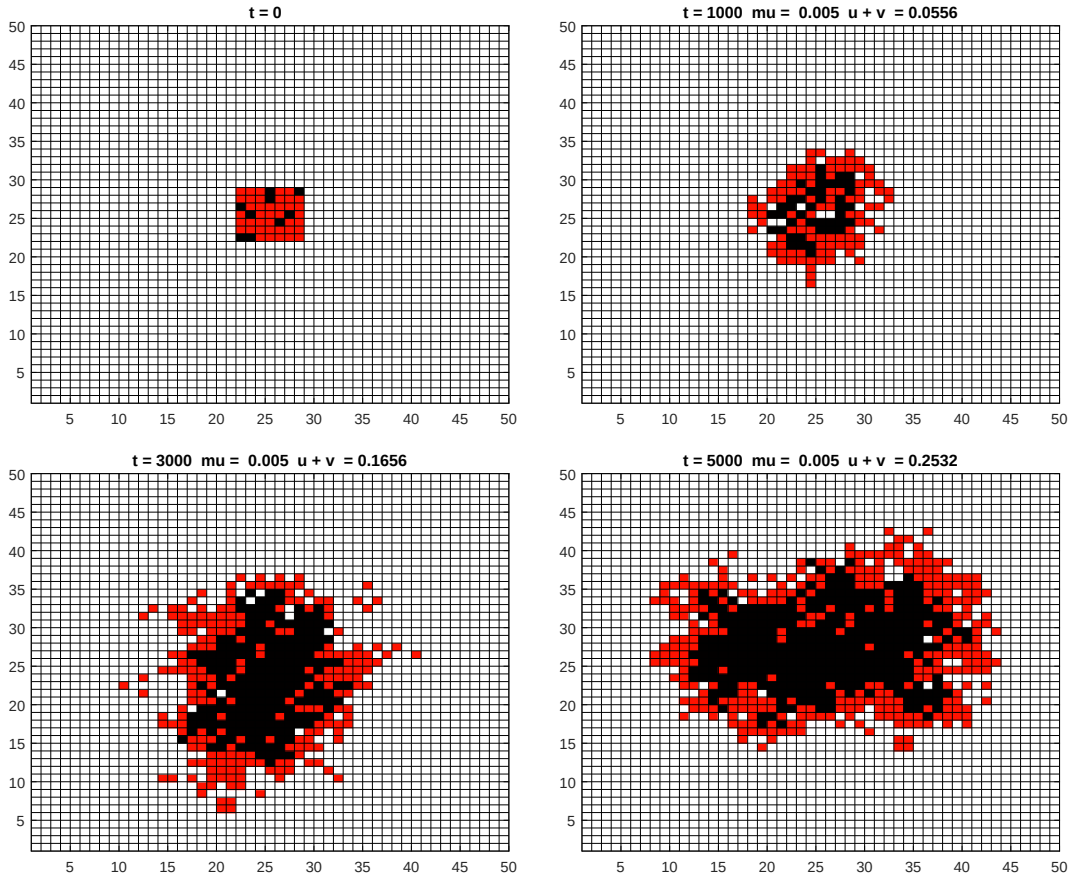

Figure 3.11: Tumor configuration at $t = 0$, $t = 1000$, $t = 3000$, and $t = 5000$. The cells colored in white are empty, while the black and red cells are occupied by CSCs and CCs respectively. $u + v$ denotes the fraction of tissue occupied by the tumour.

replication probability depends on blank spaces relatives to all the 26 cubes, that is:

$$P_r(CSC) = \frac{n_{CS}^{i,j,k}\rho_u}{26}, \tag{3.20}$$

where $n_{CS}^{i,j,k}$ is the number of safe cells and i, j, k represent the coordinates in the $\mathbb{R}^3$ space. The δ and μ parameters remain the same with the same meaning. Also ρ_v changes is role. The CC replication probability is:

$$P_r(CC) = \frac{n_{CS}^{i,j,k}\rho_v}{26}. \tag{3.21}$$

In Figure 3.12 we display the three-dimensional space with two distinct masses of tumors,

one made of CSC type cells and the other one composed by CC type cells. As we can observe the CCs tend to surround the CSCs. This 3d figure is very interesting, because it allow us to have a realistic idea of a tumor development and expansion.

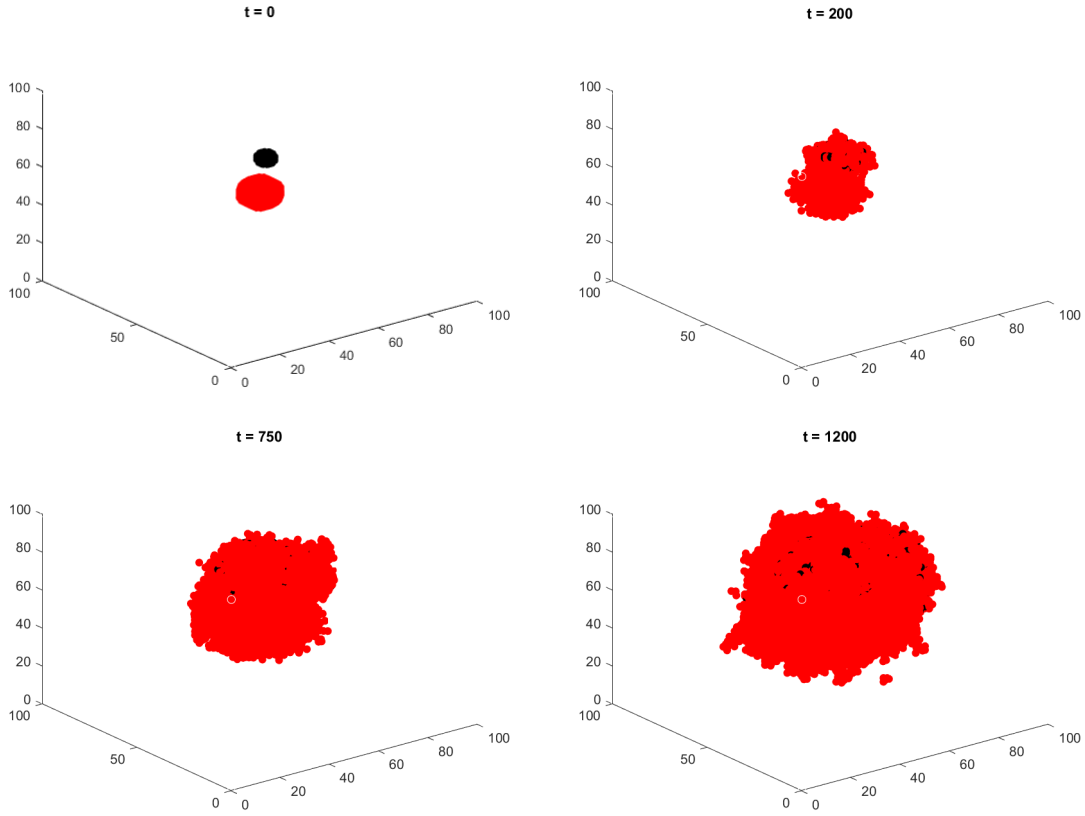

Figure 3.12: Tumor evolution in a 3d tissue of a particular initial ($t = 0$) configuration of tumour at $t = 200$, $t = 750$, $t = 1200$. The CCs (in red) tend to surround CSCs (in black).

3.3 A new mathematical model for Covid-19

At the end of 2019, a new coronavirus has been identified. It causes viral pneumonia [30] and, in very serious cases, it can bring humans to death [39]. Being a new illness, no sanitary system was really ready to counter such a disease and no state has yet vaccines. For contrasting the Covid-19 spreading, some measures has proven to be efficient. Governments, following sometimes suggestions by World Health Organization and scientific teams, closed borders, imposed the use of face masks and disinfectant, limited people social contacts closing public places like schools and cinemas, for example. Nowadays, limiting social contacts is very difficult. We have to change our lifestyles. We must be able to do smart working, for example. In all public places not too much people can be present, we must pay attention also when we take the bus or the train and so on. No public event can be organized. This means that such illness has a very deep sanitary and economic impact on our lives. For these motivations, to study the development in space and time of this new coronavirus is very important: it could be very useful to help governments in taking decisions. We just explained how unexpected was this illness in our society, so referring to previous works is not so simple. Scientific and temporal discoveries, like therapies and human first cases, are increasing everyday. Many researcher are trying to develop models in order to analyse the present situation and to predict future development of Covid-19.

To model this type of phenomena, many approaches have been proposed. The models can be deterministic or stochastic. A kind of widely adopted models are the Epidemiological ones, as the one studied by Kermack and MacKendrick [32], who proposed the Susceptible-Infected-Removed model, called the SIR model. This model has been generalized and Exposed population has been added, leading to the Susceptible-Exposed-Infected-Removed model [48]. In our opinion, the first kind of mathematical models based on dynamical equations (see [33], [34]) are extremely simplified for describing and epidemiological dynamics as in the case of the Covid-19 [31]. We consider that the SEIR model is more appropriate. It has been adopted to assess the effectiveness of measures adopted to contrast the spreading of Covid-19 and for characterizing that illness in different countries [35], [36], [37], [38]. There are also others generalization of the SEIR model, obtained by adding Quarantined and Un-quarantined populations, [35], [36]. This

extended models allow to take into account the incubation period and the period before recovery.

In this thesis, we aim to present an original model describing the evolution of the Covid-19 diffusion in a certain population, focusing particularly in the spreading of the disease in Italy in 2020. We opt to consider, in addition to Susceptible, Infected and Recovered people, Quarantined and Dead ones. Population is divided in 5 categories. As said, this coronavirus is still showing its characteristics and there are many aspect that are still unknown. However, we consider that there are different assumption which reflect the dynamic showed by this illness. Government's strategy is to discover and isolate cases, also if they are asymptomatic, by contact-tracing. Different parameters are assumed to reflect strategies and development of Covid-19, depending on time. In general we decide to use 4 parameters. The r parameter indicates the contagion index and reflects the influence of lock-down: if the whole population is isolated, it becomes close to zero. The γ constant represents the incubation period of the virus, so this value is given. We suppose that after this period an infected asymptomatic person (which corresponds to our I category) necessarily develops symptoms and therefore is quarantined (this corresponds to our Q category). No therapies are available at the moment, so someone can recover, but someone can die. The a and d parameters reflect respectively this two possibilities. By defining the parameters in an appropriate way, it is possible to see the development of Covid-19 during time from the actual state. Knowing what will happen makes possible for governments to take better decisions in time and makes also possible to prepare sanitary system for outbreaks.

3.3.1 The ODE approach

In this section we present an implementation of an ODE approach to model the covid-19 diffusion in a population. According to the assumptions described before, we

can obtain the following equations:

$$\begin{cases} S'(t) = -r\, I(t)\, S(t) \\ I'(t) = r\, I(t)\, S(t) - \gamma\, I(t) \\ Q'(t) = \gamma\, I(t) - (a+d)\, Q(t) \\ R'(t) = a\, Q(t) \\ D'(t) = d\, Q(t) \end{cases} \tag{3.22}$$

where $S(t)+I(t)+R(t)+Q(t)+D(t) = N$, being N the total population. This value can be assumed constant. Calculating the derivative of the sum $S(t)+I(t)+R(t)+Q(t)+D(t)$, which is the sum of the derivatives, and substituting their expression in (3.22), this becomes zero. So $N'(t) = 0$ and N is constant.
The meaning of the variables is the following:

- $S(t)$ represents the number of susceptible individuals at time t;
- $I(t)$ is the number of infected asymptomatic individuals at time t;
- $Q(t)$ are the quarantined individuals because they are symptomatic, at time t;
- $R(t)$ is the number of recovered individuals at time t;
- $D(t)$ represents the number of death individuals at time t;

The mechanism is represented in Figure 3.13, where we detail the classes of people and the fluxes between them.

Indeed, the parameters means:

- r is the basic reproduction number;
- γ represents how many infected asymptomatic became quarantined;
- a is the saved rate;
- d is the death rate;

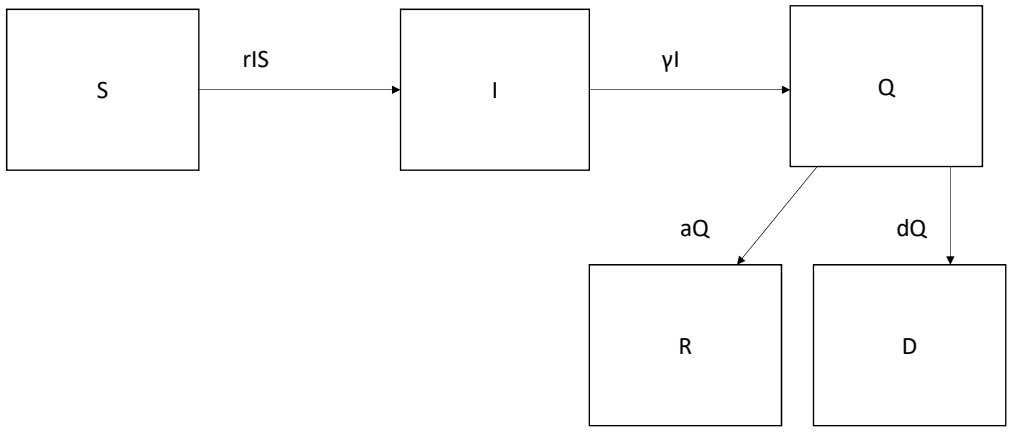

Figure 3.13: Illustration of the ODE model for Covid-19 diffusion of system (3.22).

After this description, it is possible to compare the model with the effective data, in order to show his robustness. We considered the Italian data. Choosing t_0=24/02/2020 as the beginning date of epidemic, we can set initial data as follows:

$$S(t_0) = S_0 > 0, \quad I(t_0) = I_0 > 0, \quad Q(t_0) = Q_0 \geq 0, \quad R(t_0) = R_0 > 0, \quad D(t_0) = D_0 > 0.$$

We can take the following values for defining initial data: $S_0 = 60 \times 10^6$, $I_0 = 1000$, $Q_0 = 221$, $R_0 = 30$, $D_0 = 7$. The r parameter can be chosen reflecting Italian government measures. Starting from 24/02/2020 we can take $r = 4.80 \times 10^{-9}$. Then, after having applied the first measure, r can be assumed as 2.90×10^{-9}. With the total lockdown, the r-value becomes 0.60×10^{-9}. The dates for updating r are 10/03/2020 and 23/03/03, which represent the become law of the two measures, respectively the decree #Iorestoacasa and the decree of 22/03/2020. The a, d and γ parameters are taken constant, respectively as 34.5×10^{-3}, 4.8×10^{-3} and 0.07. Under this parameters configuration, we can see in Figure 3.14 how the solutions of our ODE model satisfactorily

fit the effective datas provided by the authorities.

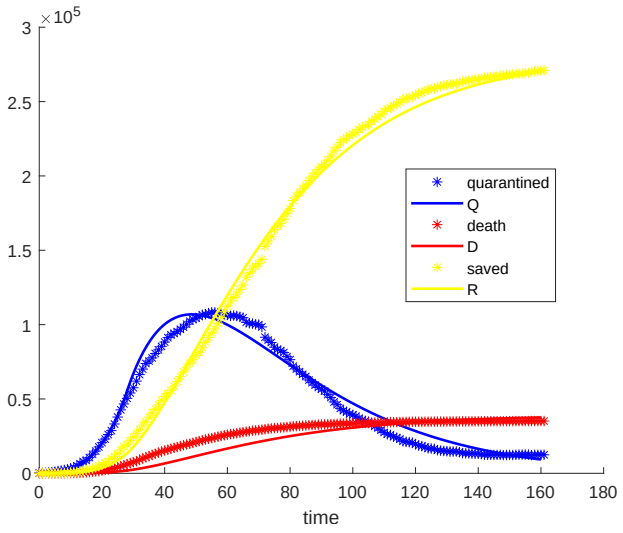

Figure 3.14: Comparision between model results and scientific data [49].

Now we aim to play with the model, also in order to make previsions. It it possible to answer the following question: what would have happened if italian government had taken social measures on different days? In Table 3.2 we report some results. We can see how many people would have died and how many would have been saved in different cases.

cases	#Iorestoacasa	decree 22/03/2020	dead population
1	10/03/2020	23/03/2020	3.7588×10^4
2	9/03/2020	22/03/2020	3.0301×10^4
3	3/03/2020	16/03/2020	8.2696×10^3
4	11/03/2020	24/03/2020	4.6610×10^4
5	16/03/2020	30/03/2020	1.6710×10^5

Table 3.2: Previsions of dead people with different time application of measures to contain the virus spread.

With this results, we can evaluate how different it can be to make a decision at different times. The first case is the real case. In second and third cases we anticipate

the measures of one day and one week respectively. From the table we can see that only one day can influence the number of dead people, with 7.287×10^4 saved people. To anticipate the measure of one week could have saved 29.3184×10^3 people. The fourth and fifth cases examine the hypothesis of a delay of one day and one week respectively. A delay of one day could be very dangerous, but a one-week delay could be a disaster. All these examples shows us how the development of an epidemic is breakable. When the situation improves since the start of spreading epidemic, government starts to open again activities and people can move. From June 3rd 2020, the population could move from one Italian region to another. Updating r to 3.5×10^{-9}, which is bigger than the value taken for the first measure, we obtain that the number of dead people will be, from the beginnig of the epidemic to one year, 6.8775×10^6. So we have to respect the rules very accurately, because it is very easy to have a big number of dead people.

3.3.2 The CA approach

As extensively discussed in this thesis, the implementation of a CA model can allow us to introduce and study the spatial effects on collective behavior. Phenomena such as the reduction of population movement or different strategies of social isolation are factors that depend on space. Clearly these characteristics cannot be described by a ODE model that shows average (over the space) values for a certain field. In this subsection we propose a model of population's behavior using a Cellular Automata approach.

To apply this method, we need a grid and a transition rule. Our grid is composed by 100×100 square cells. We can suppose that each cell represents an area of $5\,m \times 5\,m$. Therefore the total area of the whole grid can be considered as a quarter of a city. In this space there are three types of population: Susceptible, Infected (asymptomatic) and Quarantined (symptomatic) people. Susceptible and Infected can move around the surface and meet them. If an infected person meets a susceptible one, he can infect him with a certain rate. Unlike the ODE case, which is completely deterministic, we now introduce a random process for encounters as a consequence of the movement of people. Concerning the time unit we consider $1\,hour$.

A schematic representation of the CA algorithm is illustrated in Figure 3.15. The procedure involves (for each time step) going through the entire grid, for each cell:

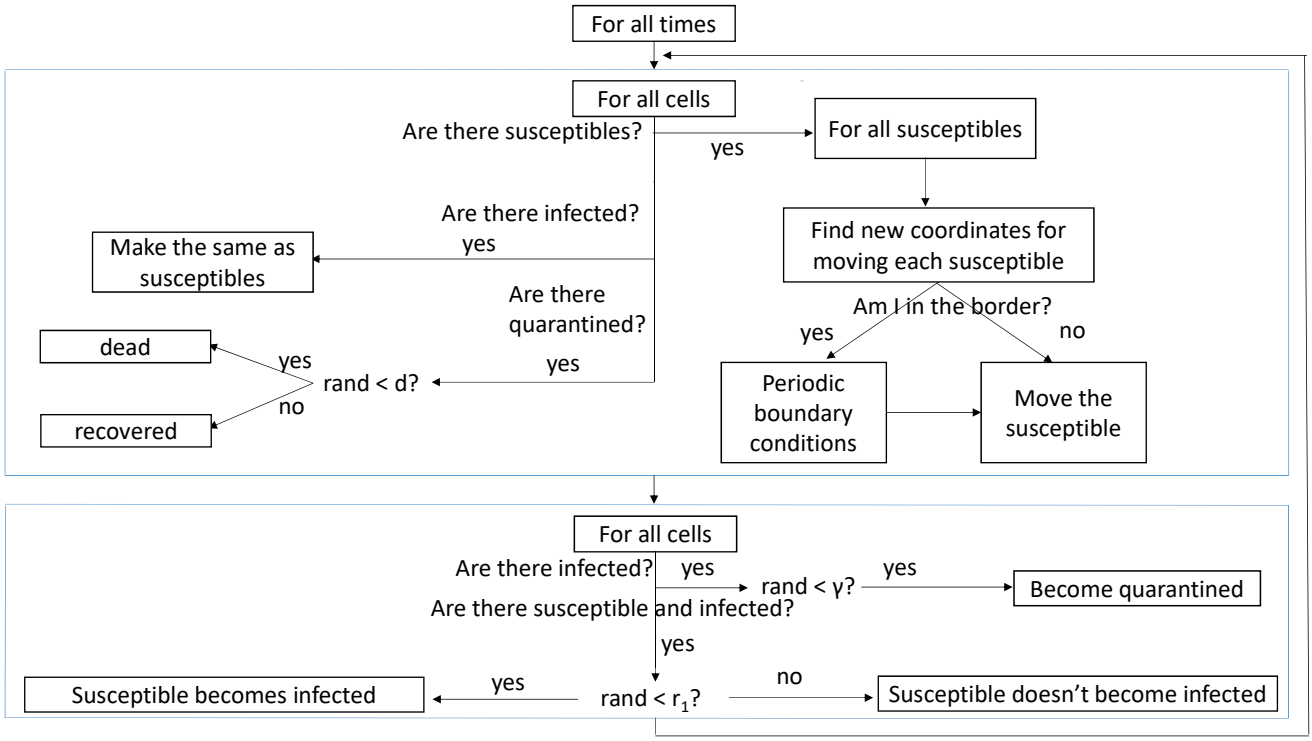

Figure 3.15: Schematic description of the algorithm for the CA approach.

- check if there are any susceptible or infected people;
- randomly decide whether to keep the person immobile or move the person in the 3×3 neighborhood;
- randomly decide, on the basis of the probability d, whether a quarantined person dies or is recovers respectively;
- randomly decide, based on the γ probability, if an infected person shows symptoms and therefore is quarantined;
- randomly decide whether a susceptible person, who is in contact (in the same cell) with an infected person, contracts the virus based on the probability r_1.

We intend to proceed with the implementation of this method and to reproduce a similar dynamic to that tested in the ODE case. For this aim, we proceeded to

redefine the parameters taking into account the different approach and the time scale. In particular, we can approximately rescale r, defining $r_1 = r \times \frac{N}{24}$, where N is the whole population and the division by 24 is due to $24h = 1day$. For the same motivation, Infected persons become Quarantined with a rate $\gamma = \gamma/24$, and Quarantined people die or recover with $d = d/24$ and $a = a/24$ rates, respectively.

In order to check the consistency of the CA model with the ODE results, we proceeded with some simulations by varying the β density of the population. We present the simulations in Figure 3.16. Each pair of figures represents a CA solution and the corresponding ODE solution. In all panels the $r = 5 \times 10^{-3}$, but we consider for the CA simulations a grid of dimensions 75×75, 100×100, and 150×150. We adopt an initial configuration of the populations as follows:

- $N = 1000$;
- $S_0 = 950$;
- $I_0 = 50$.

Having fixed the total number of people, we are facing different population densities, where the population density is given by $\beta = \frac{N}{\#\, cells}$. We get around this by multiplying the r parameter on the ODE model by the β population density. This corresponds to considering a value $r_2 = r \times \beta$.

Although the CA model is a probabilistic model, not a deterministic one like the ODE model, we obtain similar behaviors for the populations classes. We recall that in the CA scheme the rates are considered as probability to change population class. We remark finally that the simulations are consistent with respect to different population densities. Each graph of the CA model in Figure 3.16 shows the average curves of 2 tests. We conclude that, under these assumptions, the CA model is sufficiently reliable and consequently could be used to study the evolution of a population subjected to the possible infection by the virus.

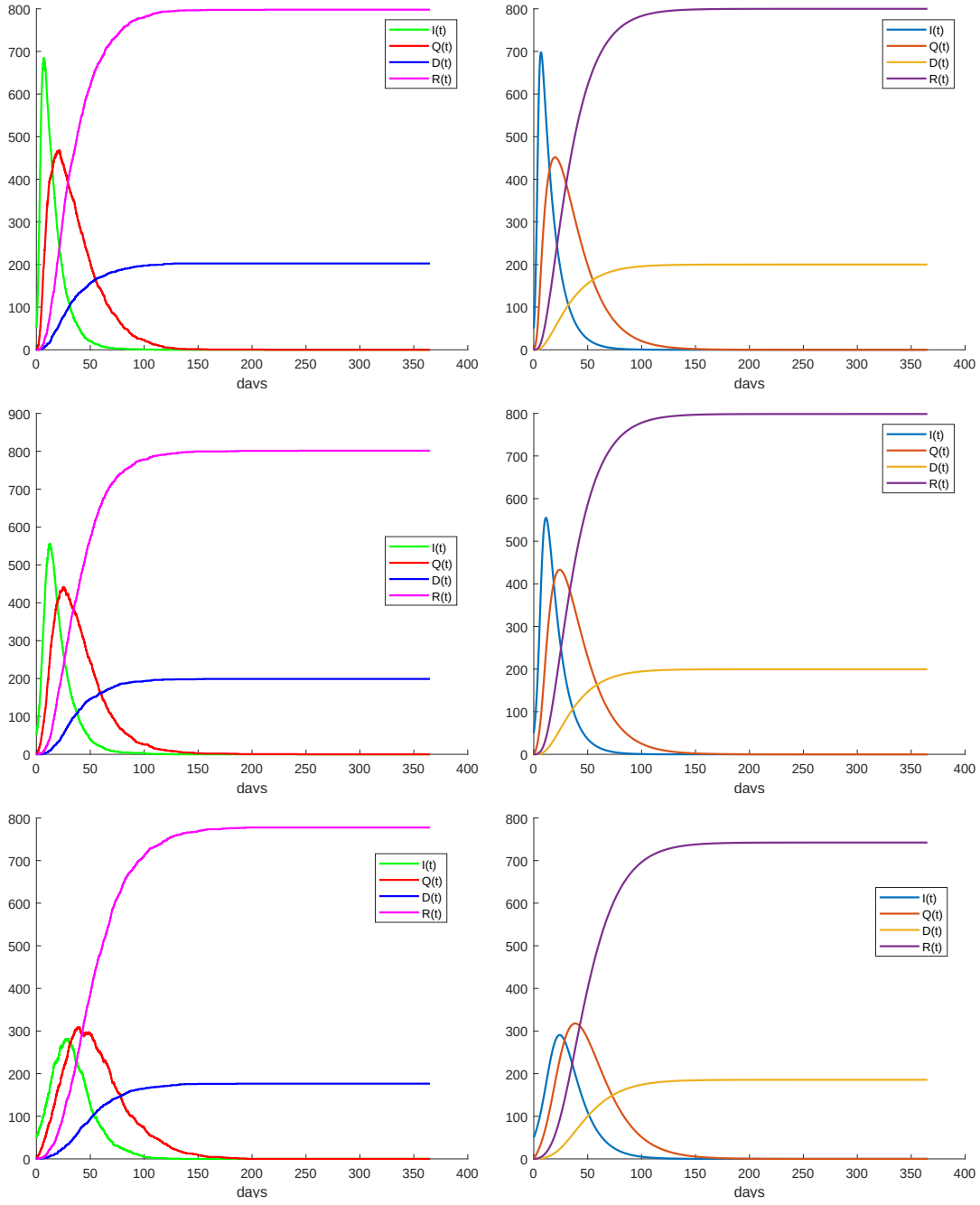

Figure 3.16: Comparison between CA solutions (on the left column) and ODE solutions (on the right column) with different grids for the CA scheme: the grid for the first CA simulation is 75×75, for the second is 100×100, and for the third is 150×150.

3.3.3 An example: four city districts

After having shown the consistency of the CA model by comparing its solutions with the ODE model, we can introduce a test where the spatial dependence is relevant.

We assume to consider 4 city districts. We suppose that our space is composed of four quarters in which susceptible and infected people can move. In each quarter we set a fixed value for r_1. In the first district we consider $r_1 = \frac{1000*3*10^{-3}}{h_0}$, in second and third quarters, which have an edge in common with the first one, $r_1 = \frac{1000*1.5*10^{-3}}{h_0}$ and in the fourth district, which has only an angle in common with the first quarter, $r_1 = \frac{1000*0.75*10^{-3}}{h_0}$, where $h_0 = 24hours$. In the first quarter we impose an initial concentration of infected $I_0 = 50$. In the other districts we assume $I_0 = 0$, which means that they are completely safe. A sketch of this test is represented in Figure 3.17.

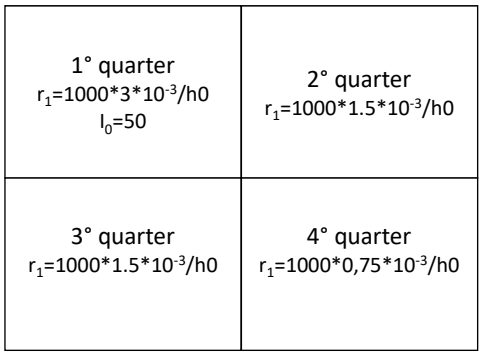

Figure 3.17: The four city districts considered in our test.

Susceptible and infected people can move from one quarter to another one. What we expect is the following situation: infected people which are in the first quarter infect much more people with respect to people in other districts, so new infected move and propagate the Covid-19 around a more safe quarter, where there are not so many infected people. This phenomena is reflected in the different amounts of quarantined and dead people in the four districts and in the delay of the infection wave in the last district, as we can see in the results of Figure 3.18.

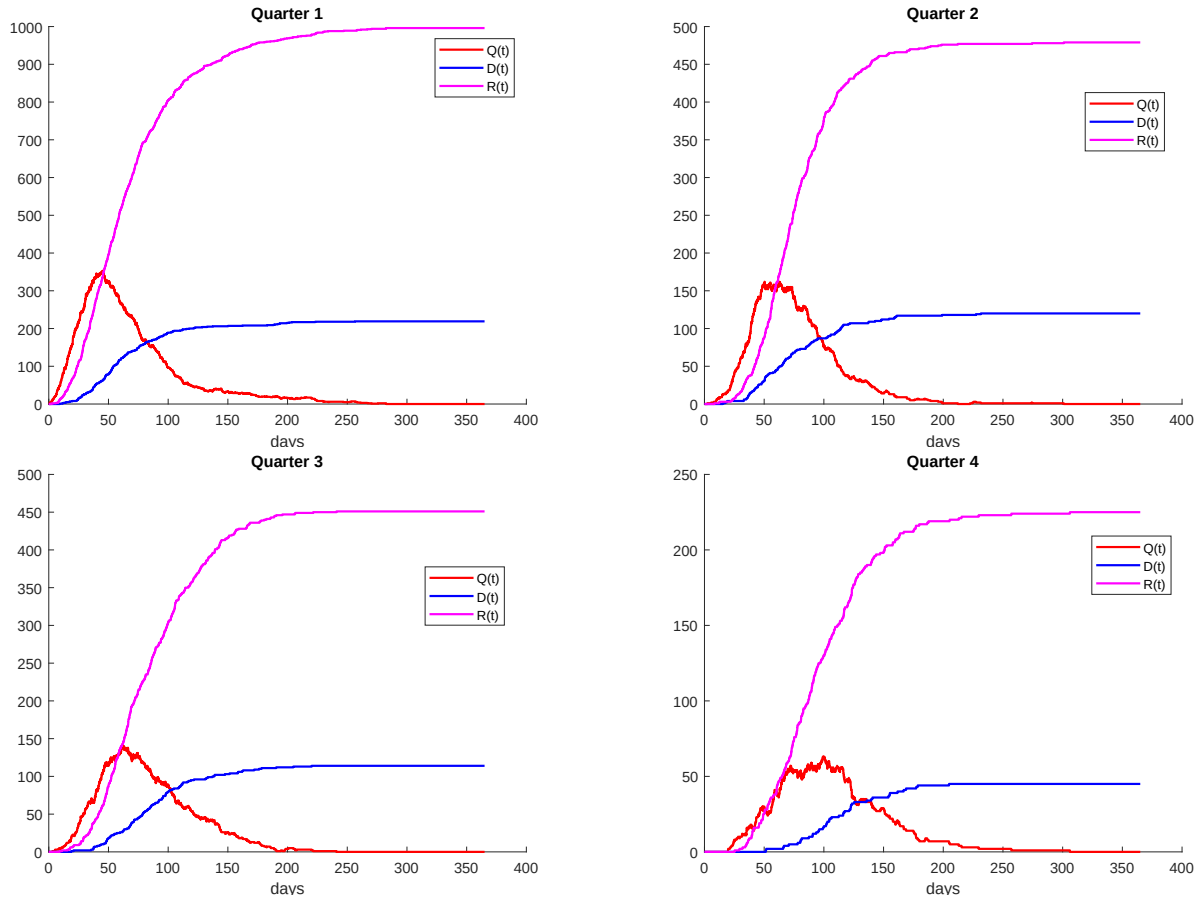

Figure 3.18: Development of Covid-19 spreading in the populations of the 4 districts (notice the different vertical scales).

Chapter 4

Numerical schemes

In this chapter we show some of the schemes written for studying our models. We used Matlab and Mathematica softwares.

4.1 Matlab schemes for the development of AD

```
k1 = 10^(-4);
k2 = 5*10^(-6);
M1 = 10^(-2);
M2 = 10^(-2);
M3 = 10^(-2);
beta=15;
dim=20;
a=zeros(dim,dim);
m=6;
a(m,m)=0.02;
x0=10*ones(dim,dim);
y0=ones(dim,dim);
z0=ones(dim,dim);
tspan=[0,180];
locale=zeros(dim,dim);
```

```
lambda0=2;
lambda=lambda0*ones(dim,dim);
lambda(6,6)=lambda0*(1-a(m,m))*(1+beta*a(m,m));
ystar=22;
theta=10^(-3);
sigma=0.05;
k=1;
a66(k)=a(m,m);
tempi(k)=0;
f1=figure;
pcolor(a)
colormap(flipud(jet))
title(['a at year ' num2str(0) ' ' ])
colorbar;
caxis([0 1]);
saveas(gcf, ['SRS_time' ,num2str(i), '.pdf']);
for T=180:180:7560
    for i=1:dim
        for j=1:dim
            inizio=[x0(i,j),y0(i,j),z0(i,j)];
            [t,y]=ode45(@(t,y)AD(k1,k2,M1,M2,M3,lambda(i,j),t,y),tspan,inizio);
            r=length(y(:,2));
            x0(i,j)=y(r,1);
            y0(i,j)=y(r,2);
            z0(i,j)=y(r,3);
            locale(i,j)=theta*subplus(y(r,2)-ystar);
            a(i,j)=a(i,j)+locale(i,j);
            lambda(i,j)=lambda0*(1-a(i,j))*(1+beta*a(i,j));
        end
    end
if mod(T,1440)==0
```

```
    f2=figure;
    pcolor(a)
    colormap(flipud(jet))
    title(['a at year ' num2str(T/360) ' ' ])
    colorbar;
    caxis([0 1]);
    saveas(gcf, ['SRS_time' ,num2str(i), '.pdf']);
end
    a66(k+1)=a(6,6);
    tempi(k+1)=T;
    k=k+1;
    tspan=[T,T+180];

end
figure(2)
plot(tempi,a66,'g');
xlabel('time')
ylabel('a(6,6)');
axis tight
```

The scheme displayed above shows how to keep track of the local development of AD, by using (3.7). First of all we define all the needed parameters and then we set initial configuration. Twice a year, so every 180 days, we cover the entire matrix representing the brain and in each REV we calculate the solution of (3.11), using the subroutine *ode*45. Then we update the value of a. We also keep track of all the a values of the cell with coordinates $(6, 6)$, in order to provide Figure 3.4. This scheme also provides Figure 3.5. Since the brain is represented as a matrix and each REV is a matrix's cell with his initial conditions, also λ, a and the inital conditions are taken as matrices.

```
\\same values for k1,k2,M1,M2,M3,beta;
dim=20;
a=zeros(dim,dim);
m=6;
```

```
a(m,m)=0.02;
x0=ones(dim,dim);
y0=20*ones(dim,dim);
z0=ones(dim,dim);
tspan=[0,180];
locale=zeros(dim,dim);
globale=zeros(dim,dim);
lambda0=2;
lambda=lambda0*ones(dim,dim);
lambda(6,6)=lambda0*(1-a(m,m))*(1+beta*a(m,m));
ystar=22;
theta=10^(-3);
sigma=0.05;
k=1;
a66(k)=a(m,m);
a86(k)=a(8,6);
a1818(k)=a(18,18);
tempi(k)=0;
sol=[x0(6,6),y0(6,6),z0(6,6)]';
f1=figure;
pcolor(a)
colormap(flipud(jet))
title(['a at year ' num2str(0) ' ' ])
colorbar;
caxis([0 1]);
saveas(gcf, ['SRS_time' ,num2str(i), '.pdf']);
for T=180:180:7560
    for i=1:dim
        for j=1:dim
            inizio=[x0(i,j),y0(i,j),z0(i,j)];
            [t,y]=ode45(@(t,y)AD(k1,k2,M1,M2,M3,lambda(i,j),t,y),tspan,inizio);
```

```
            r=length(y(:,2));
            x0(i,j)=y(r,1);
            y0(i,j)=y(r,2);
            z0(i,j)=y(r,3);
            locale(i,j)=theta*subplus(y(r,2)-ystar);
            if i==6 && j==6
                sol=[sol [x0(6,6) y0(6,6) z0(6,6)]'];
            end
        end
    end
    ag=[zeros(1,dim);a;zeros(1,dim)];
    ag=[zeros(dim+2,1) ag zeros(dim+2,1)];
    for i=1:dim
        for j=1:dim
            globale(i,j)=sigma*(subplus(ag(i,j+1)-ag(i+1,j+1))+
            subplus(ag(i+2,j+1)-ag(i+1,j+1))+subplus(ag(i+1,j+2)-ag(i+1,j+1))+
            subplus(ag(i+1,j)-ag(i+1,j+1))+subplus(ag(i,j)-ag(i+1,j+1))+
            subplus(ag(i,j+2)-ag(i+1,j+1))+subplus(ag(i+2,j)-ag(i+1,j+1))+
            subplus(ag(i+2,j+2)-ag(i+1,j+1)));
            a(i,j)=ag(i+1,j+1)+locale(i,j)+globale(i,j);
            lambda(i,j)=lambda0*(1-a(i,j))*(1+beta*a(i,j));
        end
    end
    tspan=[T,T+180];
if mod(T,1440)==0
    f2=figure;
    pcolor(a)
    colormap(flipud(jet))
    title(['a at year ' num2str(T/360) ' ' ])
    colorbar;
    caxis([0 1]);
```

```
    saveas(gcf, ['SRS_time' ,num2str(i), '.pdf']);
end
    a66(k+1)=a(6,6);
    a86(k+1)=a(8,6);
    a1818(k+1)=a(18,18);
    tempi(k+1)=T;
    k=k+1;
    tspan=[T,T+180];
end
figure(2)
plot(tempi,a66,'g');
hold on
plot(tempi,a86,'b');
plot(tempi,a1818,'r');
hold off
xlabel('time');
legend('a(6,6)','a(8,6)','a(18,18)');
axis tight
figure(3)
plot(tempi,sol(1,:),tempi,sol(2,:),tempi,sol(3,:));
xlabel('time');
axis tight
legend('X(t)','Y(t)','Z(t)');
```

This scheme allow to calculate the non-local influence of a, by using (3.9). First of all, we fix the parameters as in the case above. Then we fix the initial conditions. Also in this case some parameters are taken as constants and others as a matrices, for the same motivations above. Every 180 days, the entire matrix is covered. For each cell, the local update for a is calculated. Then our matrix is covered once again. Here, the non-local influence of each REV is calulated with (3.9) formula, using the local part already calculated. So the a-value for each REV can be updated. The solution calculated in $(6, 6)$ is saved in the vector called 'sol', in order to obtain Figure 3.8. This scheme gives

Figures 3.7 and Figure 3.6.

4.2 Matlab schemes for CSC and CC

```
mu_1=1.5;
%mu_2=0.5;
delta=0.2;
rho=0.5;
tspan = [0 50];
y0=[0.0036 0.016];
[t,y] = ode45(@(t,y)CSCCC(delta,rho,mu_1,t,y),tspan,y0);
figure(1);
plot(t,y(:,1),'r',t,y(:,2),'b');
xlabel('time')
legend('u(t)','v(t)');
sum1=y(:,1)+y(:,2);
figure(2)
plot(t,sum1,'g');
hold on
mu_2=0.5;
[t,k] = ode45(@(t,k)CSCCC(delta,rho,mu_2,t,k),tspan,y0);
sum2=k(:,1)+k(:,2);
plot(t,sum2,'y');
xlabel('time');
ylabel('u+v');
legend('mu_1','mu_2');
hold off
function dydt=CSCCC(delta,rho,mu,t,y)
dydt = [delta*y(1)*(1-y(1)-y(2));
    (1-delta)*y(1)*(1-y(1)-y(2))+rho*y(2)*(1-y(1)-y(2))-mu*y(2)];
end
```

This scheme allow to see the solution of the tumor model (3.19) and the tumor-growth paradox. As usual, first of all we set the parameters. By using the *ode*45 subroutine, this scheme plots the solution $(u(t), v(t))$ of our model, as in Figure 3.9, with different mortalities μ. Then it is possible to calculate the sum $u + v$, Figure 3.10, for verifying the tumor-growth paradox.

4.3 Mathematica scheme for stability criterion

In this section we illustrate the Mathematica scheme adopted for studying the stability of the equilibrium solution of (3.11). First, we write the system, then the jacobian matrix and the characteristic polynomial are calculated. Now, we need to isolate the a, b and c terms, in order to verify asimptotic stability using Routh-Hurwitz criterion. Finally, the Reduce command allow us to find the condition on X, Y, Z under which the inequality is verified, that is every $X > 0$, $Y > 0$, $Z > 0$. The result displayed is bigger than the one we needed. We only pay attention to the conditions described in 3.1.6. The complete scheme can be seen in the following two pages.

In[64]:=
```
X1 = -k X^2 - k X Y - ks X Z - M X + lambda
Y1 = k X^2 / 2 - k X Y - k Y^2 - ks Y Z - M * Y
Z1 = k Y^2 / 2 + k X Y - M Z
```

Out[64]= $\text{lambda} - M X - k X^2 - k X Y - ks X Z$

Out[65]= $\frac{k X^2}{2} - M Y - k X Y - k Y^2 - ks Y Z$

Out[66]= $k X Y + \frac{k Y^2}{2} - M Z$

In[67]:=
```
Jac = {{D[X1, X], D[X1, Y], D[X1, Z]}, {D[Y1, X], D[Y1, Y], D[Y1, Z]}, {D[Z1, X], D[Z1, Y], D[Z1, Z]}}
```

Out[67]= $\{\{-M - 2 k X - k Y - ks Z, -k X, -ks X\}, \{k X - k Y, -M - k X - 2 k Y - ks Z, -ks Y\}, \{k Y, k X + k Y, -M\}\}$

In[68]:=
```
JacM = MatrixForm[Jac]
```

Out[68]//MatrixForm=

$$\begin{pmatrix} -M - 2 k X - k Y - ks Z & -k X & -ks X \\ k X - k Y & -M - k X - 2 k Y - ks Z & -ks Y \\ k Y & k X + k Y & -M \end{pmatrix}$$

In[71]:=
```
pol = Simplify[Det[Jac - u * IdentityMatrix[3]]]
```

Out[71]= $-k\ ks\ X\ Y\ (M + u + k X + k Y + ks Z) - k\ ks\ (X + Y)\ \left(k\ \left(X^2 + X\ Y + Y^2\right) + Y\ (M + u + ks Z)\right) +$
$(-M - u)\ \left(k^2\ X\ (X - Y) + (M + u + 2 k X + k Y + ks Z)\ (M + u + k X + 2 k Y + ks Z)\right)$

In[72]:=
```
lista = Simplify[CoefficientList[pol, u]]
```

In[73]:=
```
{-M^3 - M^2 (3 k (X + Y) + 2 ks Z) - k ks (k (X + Y)^3 + ks Y (2 X + Y) Z) -
   M (k^2 (3 X^2 + 4 X Y + 2 Y^2) + ks^2 Z^2 + k ks (2 X Y + Y^2 + 3 X Z + 3 Y Z)),
 -3 M^2 - 6 k M (X + Y) - k^2 (3 X^2 + 4 X Y + 2 Y^2) - 4 ks M Z - ks^2 Z^2 - k ks (2 X Y + Y^2 + 3 X Z + 3 Y Z),
 -3 M - 3 k (X + Y) - 2 ks Z, -1}
```

Out[73]= $\{-M^3 - M^2\ (3 k\ (X + Y) + 2 ks Z) - k\ ks\ \left(k\ (X + Y)^3 + ks\ Y\ (2 X + Y)\ Z\right) -$
$M\ \left(k^2\ \left(3 X^2 + 4 X Y + 2 Y^2\right) + ks^2\ Z^2 + k\ ks\ \left(2 X Y + Y^2 + 3 X Z + 3 Y Z\right)\right),$
$-3 M^2 - 6 k M\ (X + Y) - k^2\ \left(3 X^2 + 4 X Y + 2 Y^2\right) - 4 ks M Z - ks^2\ Z^2 - k\ ks\ \left(2 X Y + Y^2 + 3 X Z + 3 Y Z\right),$
$-3 M - 3 k\ (X + Y) - 2 ks Z, -1\}$

In[74]:=
```
c = Expand[lista[[1]]];
b = Expand[lista[[2]]];
a = Expand[lista[[3]]];
```

In[77]:=
```
Reduce[{a * b + c > 0, X > 0, Y > 0, Z > 0, M > 0, ks > 0, k > 0}, {X, Y, Z}]
```

Out[77]=

$$
\begin{aligned}
&ks > 0 \;\&\&\\
&\Bigg(\Bigg(0 < k < \frac{ks}{9} \;\&\&\; M > 0 \;\&\&\; \Big((0 < X \le \text{Root}\big[8\,M^3 + 24\,k\,M^2\,\#1 + 24\,k^2\,M\,\#1^2 + \left(9\,k^3 - k^2\,ks\right)\#1^3\;\&,\; 1\big] \;\&\&\\
&\quad Y > 0 \;\&\&\; Z > 0\Big) \,||\, \Big(X > \text{Root}\big[8\,M^3 + 24\,k\,M^2\,\#1 + 24\,k^2\,M\,\#1^2 + \left(9\,k^3 - k^2\,ks\right)\#1^3\;\&,\; 1\big] \;\&\&\\
&\quad \Big((0 < Y < \text{Root}\big[8\,M^3 + 24\,k\,M^2\,X + 24\,k^2\,M\,X^2 + 9\,k^3\,X^3 - k^2\,ks\,X^3 +\\
&\qquad \left(24\,k\,M^2 + 44\,k^2\,M\,X + 4\,k\,ks\,M\,X + 21\,k^3\,X^2 + 3\,k^2\,ks\,X^2\right)\#1 +\\
&\qquad \left(22\,k^2\,M + 2\,k\,ks\,M + 18\,k^3\,X + 6\,k^2\,ks\,X\right)\#1^2 + \left(6\,k^3 + 2\,k^2\,ks\right)\#1^3\;\&,\; 3\big] \;\&\&\\
&\qquad Z > \text{Root}\big[8\,M^3 + 24\,k\,M^2\,X + 24\,k^2\,M\,X^2 + 9\,k^3\,X^3 - k^2\,ks\,X^3 + 24\,k\,M^2\,Y + 44\,k^2\,M\,X\,Y +\\
&\qquad 4\,k\,ks\,M\,X\,Y + 21\,k^3\,X^2\,Y + 3\,k^2\,ks\,X^2\,Y + 22\,k^2\,M\,Y^2 + 2\,k\,ks\,M\,Y^2 + 18\,k^3\,X\,Y^2 +\\
&\qquad 6\,k^2\,ks\,X\,Y^2 + 6\,k^3\,Y^3 + 2\,k^2\,ks\,Y^3 + \left(16\,ks\,M^2 + 30\,k\,ks\,M\,X + 15\,k^2\,ks\,X^2 +\right.\\
&\qquad\quad \left.30\,k\,ks\,M\,Y + 26\,k^2\,ks\,X\,Y + 2\,k\,ks^2\,X\,Y + 13\,k^2\,ks\,Y^2 + k\,ks^2\,Y^2\right)\#1 +\\
&\qquad \left(10\,ks^2\,M + 9\,k\,ks^2\,X + 9\,k\,ks^2\,Y\right)\#1^2 + 2\,ks^3\,\#1^3\;\&,\; 1\big]\big) \,||\\
&\quad \Big(Y \ge \text{Root}\big[8\,M^3 + 24\,k\,M^2\,X + 24\,k^2\,M\,X^2 + 9\,k^3\,X^3 - k^2\,ks\,X^3 +\\
&\qquad \left(24\,k\,M^2 + 44\,k^2\,M\,X + 4\,k\,ks\,M\,X + 21\,k^3\,X^2 + 3\,k^2\,ks\,X^2\right)\#1 +\\
&\qquad \left(22\,k^2\,M + 2\,k\,ks\,M + 18\,k^3\,X + 6\,k^2\,ks\,X\right)\#1^2 + \left(6\,k^3 + 2\,k^2\,ks\right)\#1^3\;\&,\; 3\big] \;\&\&\\
&\qquad Z > 0\Big)\Big)\Big)\Bigg) \,||\, \left(k \ge \frac{ks}{9} \;\&\&\; M > 0 \;\&\&\; X > 0 \;\&\&\; Y > 0 \;\&\&\; Z > 0\right)\Bigg)
\end{aligned}
$$

Chapter 5

Conclusions

In this thesis we introduced and analyzed some mathematical model conceived to study three different pathologies: Alzheimer's disease, tumor growth with stem cells and Covid-19. We described the Routh-Hurwitz criterion to study the stability of systems of autonomous ODE and several Cellular Automata schemes. With these tools we deeply analyzed the models presented, obtaining results concerning existence, uniqueness and stability of solutions. Moreover, for every model several numerical simulations were performed, also using the softwares Matlab and Mathematica, and the results reported in the thesis.

Concerning the model for Covid-19, which is a new one, given its consistency we think we are able to make some sort of forecast on the progress of the epidemic. This could be useful in choosing some strategies to be followed in the future, based on different possible scenarios.

Obviously, these models can be further developed. Some possible ideas are the following:

- check the stability of the equilibrium solution of the AD model with three different values of M;
- check what happens if, also with social distance, much people go to the same place such as school, markets and so on;
- recognize and isolate infected people as much as possible;

- examine the effect of peoplevgetting tired to be isolated and starting to go around a surface without rules;
- increase and decrease social contact for each person.

Bibliography

[1] C.Parenti, A.Parmeggiani, *Algebra lineare ed equazioni differenziali ordinarie*, Springer, 2019.

[2] S.Giostra, *Su alcuni modelli matematici per la malattia di Alzheimer*, Tesi di Laurea Magistrale Università di Bologna, a.a. 2017-2018.

[3] W.Hahn, *Stability of motion*, Springer-Verlag New York Inc. 1967.

[4] C.S.Pagnani, S.Salsa, *Analisi Matematica 2*, Zanichelli, 2016.

[5] A. Bacyinski, M. Xu, W. Wang, and J. Hu, *The paravascular pathway for brain waste clearance: current understanding, signicance and controves*, Front Neuroanat, 101, 2017.

[6] B. Plog and M. Nedergaard, *The glymphatic system in central nervous system health and disease: Past, present, and future*, Annual Review of Pathology: Mechanisms of Disease, 13, pp. 379-394, 2018.

[7] S. Fornari, A. Schaefer, M. Jucker, A. Goriely, and E. Kuhl, *Prion-like spreading of alzheimer's disease within the brain's connectome*, J. R. Soc. Interface 159, 20190356, 2019.

[8] S. Nag, B. Sarkar, A. Bandyopadhyay, B. Sahoo, VK. Sreenivasan, M. Kombrabail, C. Muralidharan, and S. Maiti, *Nature of the amyloid-monomer and the monomer-oligomer equilibrium*, J. Biol. Chem. 286, no. 16, pp. 13827-13833, 2011.

[9] J.E. Gillam and C.E. MacPhee, *Modelling amylid bril formation kinetics: Mechanism of nucleation and growth*, Journal of Physics: Condensed Matter. IOPScience 25, no. 37, 373101, 2013.

[10] R. M. Murphy and M. M. Pallitto, *Probing the kinetics of β-amyloid self-association*, J. Struct. Biol. 130, no. 2-3, pp. 109-122, 2000.

[11] M. M. Pallitto and R. M. Murphy, *Mathematical model of kinetics of β-amyloid fibril growth from the denatured state*, J. 81, no. 3, pp. 109-122, 2001.

[12] Michor F, Hughes TP, Iwasa Y, Branford S, Shah NP, Sawyers CL, Nowak MA *Dynamics of chronic myeloid leukaemia*, Nature 435(7046), pp.1267–1270, 2005.

[13] Borsi I, Fasano A, Primicerio M, Hillen T, *A non-local model for cancer stem cells and the tumour growth paradox*, Math Med Biol 34(1), 2005.

[14] M.Bertsch, B.Franchi, L.Meacci, M. Primicerio, M.C.Tesi, *The amyloid cascade hypothesis and Alzheimer's disease: a mathematical model*, European journal, 2020.

[15] R.J O'Brien, P.C. Wong,*Amyloid precursor protein processing and Alzheimer's disease*, Annual Review of Neuroscience 34, pp. 185-204 (English (US)), 2011.

[16] S. Chimon, M.A. Shaibat, C.R. Jones, D.C. Calero, B. Aizezi, and Y. Ishii, *Evidence of fibril like β-sheet structures in a neurotoxic amyloid intermediate of Alzheimers β-amyloid*, Nature Structural and Molecular Biology 14, no. 12, pp. 1157-1164, 2007.

[17] K. Ono, M. M. Condron, and D. B. Teplow, *Structure-neurotoxicity relationships of amyloid β-protein oligomers*, P. Natl. Acad. Sci. USA 106, no. 35, pp. 14745-14750, 2009.

[18] E. Karran, M. Mercken, and B. De Strooper, *The amyloid cascade hypothesis for Alzheimer's disease: an appraisal for the development of therapeutics*, Nat Rev. Drug Discov. 10, no. 9, pp. 698-712, 2011.

[19] W.S.T. Griffinn, J.G. Sheng, M.C. Royston, S.M. Gentleman, J.E. McKenzie, D.I. Graham, G.W. Roberts, and R.E. Mrak, *Glial-neuronal interactions in Alzheimer's*

disease: the potential role of a cytokine cycle in disease progression, Brain Pathol. 8, no. 1, pp. 65-72, 1998.

[20] T. A. Good and R. M. Murphy, *Effect of β-amyloid block of the fast-inactivating K^+ channel on intracellular Ca^{2+} end excitability in a modeled neuron*, P. Natl. Acad. Sci. USA 93, pp. 15130-15135, 1996.

[21] D. Selkoe, J. Hardy, *The amyloid hypothesis of Alzheimer's disease at 25 years*, EMBO Molecular Medicine, vol 8, no 6, 2016.

[22] A. C. Fowler, *Mathematical Models in the Applied Sciences*, Cambridge University Press, 1998.

[23] A. Adamatzky, *Game of Life Cellular Automata*, Vol. 1, London: Springer, 2010.

[24] *https://www.fondazioneveronesi.it/magazine/tools-della-salute/glossario-delle-malattie/alzheimer-2#section-0*

[25] M.Mitchell, *Computation in Cellular Automata: A Selected Review*, SFI Working papers, pgg. 95-140, 2005.

[26] S. Wolfram, *Statistical mechanics of cellular automata*, Review of modern physics 55.3, 1983: 601.

[27] S. Wolfram, *A new kind of science*, Vol 5, Champaign, IL: Wolfram media, 2002.

[28] L. Meacci, M. Primicerio, *Mathematical models for tumors with cancer stem cells*, Computational and Applied Mathematics 37.5, pp. 6544-6559, 2018.

[29] L. Meacci, D. de Oliveira Medeiros, G. C. Buscaglia, M. Primicerio, *O paradoxo do crescimento tumoral atraves de um modelo 3d de automatos celulares com celulas-tronco cancerıgenas*, C.Q.D – Revista Eletronica Paulista de Matematica 14, Edi¸cao Ermac, pp. 132–146, 2019.

[30] D. McGonagle, K. Sharif, A. O'Regan, C. Bridgewood, *The Role of Cytokines including Interleukin-6 in COVID-19 induced Pneumonia and Macrophage Activation Syndrome-Like Disease*, Autoimmunity Reviews, Volume 19, Issue 6, Elsevier, 102537, June 2020.

[31] J. Zhang, K. Ma, H. Li, M. Liao, W. Qi, *The continous evolution and dissemination of 2019 novel human coronavirus*, Journal of Infection 80 (6), pp. 671-693, 2020.

[32] S. Flexman, S. Mishra, A. Gandy, H. J. T. Unwin, T.A. Mellan, H. Coupland, C. Whittaker, H. Zhu, T. Berah, J. W. Eaton et al, *Estimating the effect of non-pharmaceutical interventions on Covid-19 in europe*, Nature, pp. 1-5, 2020.

[33] L. Manganoni, M. Pistilli, *Epidemic analysis of Covid-19 in Italy by dynamical modelling*, preprint, SSRN 3567770, 2020.

[34] S. H. White, A. M. Del Rey, G. R. Sànchez, *Modelling epidemics using cellular automata* Applied mathematics and computation, 186 (1), pp. 193-202, 2007.

[35] S. Wolfram, *A new kind of science*, Vol. 5, Wolfram media Champaign, IL, 2002.

[36] G. E. Box, *Science and statistics*, Journal of the American Statistical Association 71 (356), pp. 791-799, 1976.

[37] T. Colbourn, *Covid-19: extending or relaxing distancing control measures*, The Lancet Public Healt 5 (5), pp. e236-e237, 2020.

[38] L. Lopez, X. Rodó, *A Modified SEIR mode to Predic the COVID-19 Outbreak in Spain and Italy: Simulating Control Scenarios and Multi-Scale Epidemics*, SSRN, 29 April 2020.

[39] Li, Geng, et al., *Coronavirus infections and immune responses*, Journal of medical virology 92.4, pp. 424-432, 2020.

[40] Y. Achdou, B. Franchi, N. Marcello, M.C. Tesi, *A qualitative model for aggregation and diffusion of β-amyloid in Alzheimer's disease*, Journal of Mathematical Biology, Vol.67, pp 1369-1392, 2013.

[41] M. Bertsch, B. Franchi, M.C. Tesi, A. Tosin, *Well-Posedness of a mathematical model for Alzheimer's disease*, SIAM Journal on Applied Mathematics, Vol 50, No. 3, pp. 2362-2388, 2018.

[42] A. Alzheimer, *Ueber den Abbau des Nerwengewebes*, Allg. Ztsxhr. f. Psychiat, 1906.

[43] L. Edelnstein-Keshet and A. Spiross, *Exploring the formation of Alzheimer's disease senile plaques in silico*, J. Theor. Biol. 216, no.3, pp. 301-326, 2002.

[44] C. D. Pagani, S. Salsa, *Analisi Matematica*, Vol. 1, Masson, pag 229, 1995.

[45] R. Betteridge, M.R. Owen, H.M. Byrne, T.Alarcón, P. K. Maini, *The impact of cell crowding and active cells movement on vascular tumor growth*, Netw Heterog Media 1(4), pp 515-535, 2006.

[46] I. Borsi, A. Fasano, M. Primicerio, T. Hillen, *A non-local model for cancer steam cells and the tumor growth paradox*, Math Med Biol 34(1), pp. 59-75, 2015.

[47] H. Enderling, A. R. Anderson, M. A. Chaplain, A. Beheshti, L. Hlatky, P. Hahnfeldt, *Paradoxical dependencies of tumor dormancy and progression on basic cell kinetics*, Cancer Res 69(22), pp. 8814-8821, 2009.

[48] F. Brauer, P. van den Driessche, J. Wu, *Mathematical Epidemiology*, Springer, 2008.

[49] Data coming from Italian Protezione Civile.

Acknowledgemets

Desidero ringraziare in primo luogo la professoressa Maria Carla Tesi. La ringrazio per avermi fatto tanto appassionare a questi argomenti, per avermi sempre ascoltato, per avermi detto dei semplici si o dei semplici no quando avevo delle buone o cattive idee. La ringrazio anche, e soprattutto, per avermi fatto tanto divertire durante l'elaborazione di questa tesi. La ringrazio un po' per la persona che è.

Ringrazio il dott. Luca Meacci, per avermi aiutato a redigere una tesi a prova di pandemia, fuso orario, improbabili trasferimenti di ufficio, computer che si arrendono, portoghese, italiano, toscano e inglese. Che peccato dover fare le chiamate alle 21!

Ringrazio i miei genitori, per gli innumerevoli sacrifici fatti e per la fiducia che hanno in me.

Ringrazio il Tiffany's fan club, grazie a voi conserverò un bellissimo ricordo di questi anni. Un pensiero particolare va a Laura, per avermi supportato (e sopportato) nelle ultimissime (e scocciantissime) sconfitte.

Ringrazio me stessa per la tenacia e la pazienza che ho e che ho avuto in questi anni. Mi ringrazio anche per aver saputo cambiare strada quando era il momento. Spero di riuscire sempre a far uscire il meglio di me nella mia vita.

Infine, il mio ringraziamento più sentito e più profondo va alla piccola Popia, per avermi fatto cambiare punto di vista sul mondo.